10

HYDROXYAPATITE NANOMATERIALS: SYNTHESIS, PROPERTIES, AND FUNCTIONAL APPLICATIONS

Yushen Lu[*,†,a], Wenkai Dong[*,†,a], Junjie Ding[*,‡,a], Wenbo Wang[*,a], Aiqin Wang[*]

[*]Key Laboratory of Clay Mineral Applied Research of Gansu Province, Center of Eco-material and Green Chemistry, Lanzhou Institute of Chemical Physics, Chinese Academy of Sciences, Lanzhou, People's Republic of China, [†]Center of Materials Science and Optoelectronics Engineering, University of Chinese Academy of Sciences, Beijing, People's Republic of China, [‡]School of Materials Science and Engineering, Lanzhou Jiaotong University, Lanzhou, People's Republic of China

10.1 Structure and Physicochemical Properties of Hydroxyapatite (HAP)

The crystal structure of HAP belongs to the hexagonal system, with the chemical formula $Ca_{10}(PO_4)_6(OH)_2$, the space group $P63/m$, and the unit cell parameters of $a=b=0.942$ nm, $c=0.688$ nm, $\alpha=\beta=90$ degrees, $\gamma=120$ degrees. The crystal structure model of HAP is shown in Fig. 10.1 [1]. As is shown, Ca^{2+} ions occupied two different positions in the unit cell. Four calcium atoms vertically distributed along the *c*-axis are called Ca(I), and the six calcium atoms arranged in a positive triangle around the *c*-axis are called Ca(II) [2,3]. Ca(I) is located at $c=0$ and $c=1/2$, which form a coordination polyhedron with the oxygen atoms in the surrounding nine PO_4^{3-} groups. Ca(II) occupies the positions of $c=1/4$ and $c=3/4$, and there are seven oxygen atoms around it, which are derived from six PO_4^{3-} groups and one OH^- group, respectively. PO_4^{3-} group has P as the central atom and four oxygen atoms coordinated to form a regular tetrahedral structure. OH^- is located at the center of an equilateral triangle formed by Ca and O perpendicular to the *c*-axis and at the four

[a] These authors contributed equally to this chapter.

Nanomaterials from Clay Minerals. https://doi.org/10.1016/B978-0-12-814533-3.00010-7

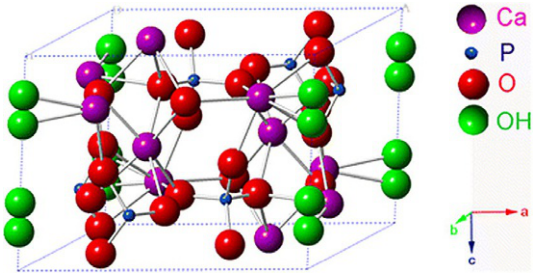

Fig. 10.1 Crystal structure of HAP. Reproduced with permission from M. Qi, K. He, Z. Huang, R. ShahbazianYassar, G. Xiao, Y. Lu, T. Shokuhfar, Hydroxyapatite fibers: a review of synthesis methods, J. Oral Maxillofac. Surg. 69 (8) (2017) 1354–1360.

corners of the crystal structure [4]. Ca(I) and Ca(II) are co-topped or coplanar with PO_4^{3-} tetrahedron, so that the structure of HAP has better stability.

HAP is the most stable phase among calcium phosphate materials [5], with a density of 3.156 g/cm^3, a melting point of 1650°C, a refractive index of 1.64 to 1.65, a Mohs hardness of 5, and a moderate hardness. HAP is slightly soluble in water, and the solubility constant at 37 °C is 58.65, which is easily soluble in acid while difficult to dissolve in alkali. HAP has strong ion exchange capacity, and Ca^{2+}, OH^-, $(PO_4)^{3-}$ in the crystal structure can be replaced by various ions in an unnecessary way [6]. For example, Ca^{2+} is easily replaced by metal ions such as Zn^{2+}, Cu^{2+}, Sr^{2+}, Ba^{2+}, Cd^{2+}, Hg^{2+}, Na^+, Ag^+, and the OH^- position is a channel ion position, which is easily replaced by halogen ions such as F^-, Cl^-, and Br^-. $(PO_4)^{3-}$ may also be substituted by an acid ion such as CO_3^{2-} or SiO_4^{4-}. Each substitution affects the unit cell parameters of HAP, which in turn affects its crystallinity, thermal stability, structural stability, micromorphology, other physicochemical properties, and biological properties. This also provides new ideas for the modification of HAP and expands its application range.

10.2 Synthesis of Hydroxyapatite

HAP is the main mineral component in the bones and teeth of mammals. It has been confirmed that its nanoparticles can observably enhance the biocompatibility and bioactivity of artificial biomaterials. Over the past decades, HAP has increasingly received attention. Many researchers are passionately developing more synthesis ways with the advantages of low cost and simple operation (Fig. 10.2). Several vital physicochemical properties and experimental parameters usually are considered for the preparation of HAP, such as the aggregations of nanoparticles, low purity, amorphous crystal phase, and precise control of morphology. Aiming at these problems, some developments also are achieved, including developing new kinds of synthesis techniques and optimizing experimental conditions. Of course, as a whole, there are always corresponding advantages and disadvantages for each method; thus it may depend on the practical needs to select synthesis methods and experimental parameters [7].

In general, the nanoparticles with various morphologies and sizes have different properties. So, nanosized HAP exhibits better morphology and crystallinity, suitable stoichiometry and high purity, and received much more attention. Based on this, many researchers focused on the preparation of HAP in various sizes and shapes by employing a series of traditional and/or new methods, e.g., typical hydrothermal, chemical precipitation, solid state synthesis, electrospinning,

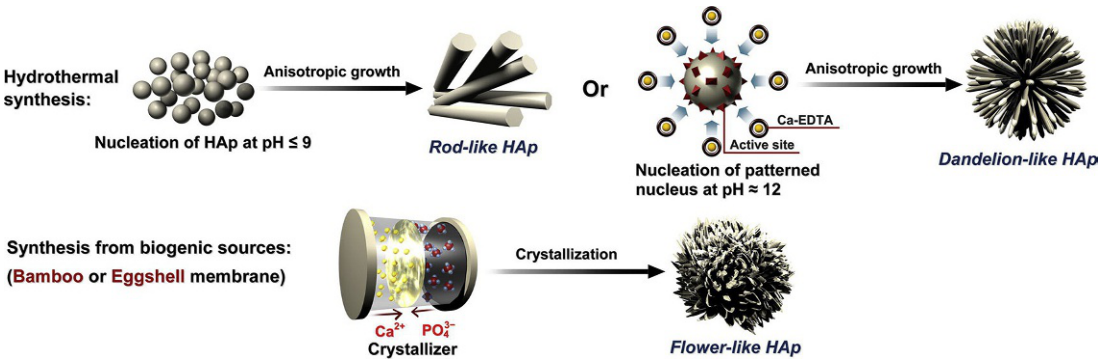

Fig. 10.2 Synthesis methods of HAP with different morphologies. Reproduced with permission from M. Sadat-Shojai, M.T. Khorasani, E. Dinpanah-Khoshdargi, A. Jamshidi, Synthesis methods for nanosized hydroxyapatite with diverse structures, Acta Biomater. 9 (8) (2013) 7591–7621.

microwave irradiation, chemical vapor, and so on. To date, a large number of HAP with specific morphologies, such as sphere, rod, needle, tube, fiber, sheet, bundles of nanorods, flower and bowknot, have been synthesized successfully, and their possible applications in relevant fields have also been evaluated [8,9]. Liu et al. employed a simple and economic hydrothermal process to prepare HAP powder with needle morphology, and the needle-shape grain possessed 130–170 nm in length as well as 15–25 nm in width. The as-prepared HAP powder can be heated to get a high density at 1200–1300°C without occurrence of decomposition in this process. The ceramic suitably sintered possessed a pore-free surface structure, which simultaneously exhibited a high flexural strength (120 MPa), a tough micro-Vickers hardness (5.1 GPa), and the better fracture toughness (1.2 MPa·m^{12}) [10].

On the whole, the synthesis methods of HAP can be classified as dry method, wet method, high-temperature treatment, and combination method. Specifically, dry methods include solid-state and mechanochemical methods; wet methods include chemical precipitation, hydrolysis, sol-gel, hydrothermal, emulsion, and nonchemical, which is commonly used in synthesis of HAP. It is worth noting that chemical precipitation and hydrothermal methods are the most well-known among those methods. Comparatively, the combination methods such as hydrothermal-mechanochemical, hydrothermal-hydrolysis, and hydrothermal-microemulsion methods have advantages aimed at some particular situations. Here, we emphatically introduce several classical methods, including chemical precipitation, hydrothermal, combination routine, sol–gel, microemulsion, and mechanochemical methods.

10.2.1 Mechanochemical Method

Mechanochemical method is a commonly used dry method for the fabrication of various nanomaterials, such as nanocrystalline

alloys and ceramics [11,12]. The heterogeneous particles with a well-defined structure can be prepared by the mechanochemical method because the presence of surface-bonded species resulting from pressure may improve the thermodynamic and kinetic reactions between particles [13–16]. In a typical mechanochemical reaction process, the materials are ground with a planetary mill with an optimizing stoichiometric molar ratio of reactants [17,18]. The main implement variables include the type of raw materials, the milling medium, milling time, milling speed, and so on [17,19]. The relevant reaction routes are described as follows:

$$10CaCO_3 + 6(NH_4H_2PO_4) \rightarrow Ca_{10}(PO_4)_6(OH)_2 + 8H_2O + 10CO_2 + 6NH_3 \quad (10.1)$$

$$3Ca_3(PO_4)_2 \bullet xH_2O + Ca(OH)_2 \rightarrow Ca_{10}(PO_4)_6(OH)_2 + xH_2O \quad (10.2)$$

$$9CaO + Ca(OH)_2 + 3P_2O_5 \rightarrow Ca_{10}(PO_4)_6(OH)_2 \quad (10.3)$$

As mentioned above, HAP particles prepared by a typical dry method always keep a large size and disorder morphology. Comparatively speaking, wet methods are favorable to produce HAP with a nanoscale structure and regular morphology, exhibiting a more popular tendency among numerous researchers. Classical chemical synthesis processes of HAP for wet methods are concluded as follows:

$$10Ca(NO_3)_2 + 6(NH_4)_2HPO_4 + 8NH_4OH \rightarrow Ca_{10}(PO_4)_6(OH)_2 + 20NH_4NO_3 + 6H_2O \quad (10.4)$$

$$10Ca(NO_3)_2 + 6(NH_4)_3PO_4 + 2H_2O \rightarrow Ca_{10}(PO_4)_6(OH)_2 + 18NH_4NO_3 + 2HNO_3 \quad (10.5)$$

$$10Ca(NO_3)_2 + 6H_3PO_4 + 2NH_4OH \rightarrow Ca_{10}(PO_4)_6(OH)_2 + 2NH_4NO_3 + 18HNO_3 \quad (10.6)$$

$$10Ca(OH)_2 + 6H_3PO_4 \rightarrow Ca_{10}(PO_4)_6(OH)_2 + 18H_2O \quad (10.7)$$

$$10CaCl_2 + 6(NH_4)_2HPO_4 + 8NH_4OH \rightarrow Ca_{10}(PO_4)_6(OH)_2 + 20NH_4Cl + 6H_2O \quad (10.8)$$

$$10CaCO_3 + 6(NH_4)H_2PO_4 + 2H_2O \rightarrow Ca_{10}(PO_4)_6(OH)_2 + 3(NH_4)_2CO_3 + 7H_2CO_3 \quad (10.9)$$

$$10CaSO_4 \bullet 2H_2O + 6(NH_4)_2HPO_4 \rightarrow Ca_{10}(PO_4)_6(OH)_2 + 3(NH_4)_2SO_4 + 7H_2CO_3 \quad (10.10)$$

10.2.2 Chemical Precipitation

Chemical precipitation is a conventional and simple method to prepare HAP. Under the condition of normal temperature and pH 4.2, HAP has a low solubility and stable CaP phase was formed in the aqueous solution [20–25]. Nevertheless, the precipitation reaction is commonly performed with a higher pH values and elevating temperatures until the boiling point of water [26,27]. Many typical calcium and phosphate chemicals can be used to synthesize HAP by a chemical precipitation reaction, such as calcium hydroxide, calcium chloride, calcium nitrate and orthophosphate, phosphate salts, and so on. In addition, the dropwise addition operation is also necessary with the Ca/P molar ratio of 1.67 [28–31]. At last, the obtained suspension is usually subjected to an Ostwald ripening process under the atmospheric pressure [32,33]. However, the HAP synthesized by the chemical precipitation method is always non-stoichiometric, weakly crystalline, and no regulation [34–36]. Many factors are considered regarding these drawbacks, including the high chemical affinity of HAP with some ions, the complex compositions of the CaP compounds, the H-bond interaction between HAP, and the uncertain kinetic parameters [37,38]. Therefore, precise control over the experimental conditions is usually required for the preparation of HAP with minimum defects. Indeed, to get a single-crystal HAP with well purity, the precipitation process should always be performed with a high pH or a high temperature, or both.

Gibson et al. [39] first prepared the bioceramic via incorporating a small amount of silicon into the HAP by using a chemical precipitation method. During this process, a single-phase silicon-substituted HAP (Si-HAP) was obtained via calcining the as-prepared silicon-substituted apatite (Si-Ap) at 700°C, and thus no secondary phases, e.g., tricalcium phosphate or calcium oxide, were found in the product. However, the silicon substitution in HAP changed the lattice parameters. This substitution also contributed to a decline toward the quantities of hydroxyl groups located in the unit cell.

Tas [40] synthesized the nanosized (~50 nm) ceramic powder of calcium HAP with a homogeneous and high-purity phase by using calcium nitrate and diammonium hydrogen phosphate mixed in synthetic body fluid (SBF) via the chemical precipitation process. The prepared precursor was found to readily reach a purity >99% after 6 h of sintering in normal atmosphere at 900°C. The result showed that no decomposition occurred for HAP in this process, especially for the undesired β-TCP phase.

10.2.3 Hydrothermal Methods

As one of the most usual ways for the synthesis of HAP, the hydrothermal method is commonly achieved via treating the mixture of reactants under a high temperature and pressure environment in an

autoclave or pressure-resistant reactor [41–45]. It has been confirmed that HAP nanoparticles prepared by using the hydrothermal method show regular stoichiometric and are highly crystalline [46–48]. What is more, phase purity and Ca/P ratio of HAP observably enhance with the increment of hydrothermal reaction temperature. But, a relatively higher temperature and pressure need more expensive synthesis cost, which is also a notable trait compared to other methods. Hydrothermal method has been used to prepare 1D nanosize HAP, attributed to its priority to induce growth of HAP along 1D orientation. It is generally implied that the generation of rod-like crystals in the hydrothermal reaction process includes two main steps, nucleation and growth step, in which small crystalline nuclei are formed in a supersaturated reactants solution, and the nuclei gradually grows until forming the final structure and morphology [49,50]. Liu et al. [51] synthesized the HAP by using a simplified hydrothermal method. In this process, $Ca(OH)_2$, $Ca(H_2PO_4)_2{\cdot}H_2O$, and deionized water were heated in a high-pressure pot at 109°C for 1–3 h. The resultant product has a well crystalline degree, specific surface area of 31–43 m^2/g, and CaP ratio of 1.640–1.643. During the hydrothermal reaction process, temperature and pH are the most important factors affecting the shape and size of HAP nanoparticles. Moreover, the high pH value will contribute to an isotropic or weak-anisotropic growth, so that the crystal can grow to form spherical nanoparticles. However, the most evident disadvantage of the hydrothermal method is the feeble ability to control the size distribution of nanoparticles.

Microwave heating hydrothermal reaction has also been applied to fabricate interconnective porous structured bodies by foaming as-synthesized calcium-deficient HAP (Ca-deficient HAP) precipitates containing H_2O_2. The porous bodies were sintered by a microwave process with activated carbon as the embedding material to prepare nano- and submicron-structured ceramics. The study results suggest that porous carbonated biphasic CaP ceramics with a nanostructure promote osteoblast adhesion, proliferation, and differentiation [52].

10.2.4 Sol-Gel Methods

The sol-gel method offers the superiority of chemical reaction at molecular level, which is favorable to improve the chemical homogeneity of the obtained products [53–56]. In addition, the low temperature atmosphere of the reaction process is another advantage of the sol-gel method. Among other wet methods, the temperature exceeding 1000°C is commonly needed to calcine HAP crystals, while the temperature of several hundred degrees or even lower is required for sintering of HAP via the sol-gel way. In addition, the nanoparticles prepared by using this method commonly perform a stoichiometric

structure with large specific surface area and small size distribution [57–60]. According to the in vitro experiment results, the biocompatibility of HAP prepared by sol-gel method is better than the HAP prepared by other ways [61]. However, this method also has some disadvantages such as the formation of the secondary phase (e.g., calcium oxide) during the reaction process and the expensive cost of some raw materials (e.g., alkoxide precursors). It is worth noting that the secondary calcium oxide phase is adverse to the biocompatibility of HAP, and thus attempts have been made to remove calcium oxide through washing the calcined product using a dilute hydrochloric acid solution or prolonging the ripening time [62–64]. The traditional sol-gel method involved the preparation of a 3D structure by mixing alkoxides in an aqueous or organic phase, followed by ripening, gelation, drying, and finally removing organics from the resultant product by heat treatment [65–67]. In the solution, the reaction between the calcium and phosphorus reactants occurs slowly, and this is the reason why a long period of ripening is commonly required. What is more, the heat-treatment process has been found to be vital for the formation of pure HAP and the removal of residual organics from the porous gel [54–56,68,69]. It is worth noting that the formation rate of gelation, type of the solvent, temperature, and pH applied in the sol–gel synthesis process extremely depend on the chemical nature of the reactants.

Liu et al. [70] synthesized HAP powders by a sol-gel technique using triethyl phosphite and calcium nitrate as phosphorus and calcium precursors, respectively. The resultant sols were stable, and no gelling existed in the ambient environment for more than 5 days, which would become gel after the evaporation of the solvents. X-ray diffraction demonstrated that the structure of HAP first appears at a temperature of 350°C, whose crystal size and content both increased as increment of sintering temperature. In addition, the distinction of initial diluting media (water and anhydrous ethanol) did not affect the morphology and crystalline degree of the resultant HAP powder.

10.2.5 Emulsion Synthesis Method

The precise control over shape, size, and scale distribution of particles is crucial and fairly difficult, especially when preparing the nanosize material with fewer agglomerations. Emulsion synthesis method was employed to synthesize HAP nanoparticles, which may deal with the aggregation problem and restrict the generation of violent clustering [71]. Nevertheless, at present, this method exhibits a tremendous superiority not only to synthesize homogeneous ceramic nanoparticles, but also to control the microstructure and size of resultant powder. Indeed, among many wet synthesis methods of HAP, microemulsion

is demonstrated to be more effective to create a uniform particle size, control the particular morphology, and reduce the aggregation of HAP particles [72–75]. Moreover, a mild synthesis process with no need of high temperature or harsh pressure makes the emulsion technique a promising method to synthesize HAP. Microemulsion possesses a thermo-dynamical stability and isotropic dispersion of two immiscible liquid phases (i.e., water phase and oil phase) commonly stabilized via the presence of surfactants. Surfactants are amphiphilic matters with a hydrophilic end and a hydrophobic group in the tail part, which may lead to formation of a dispersed phase with nanometer regimes; the formed emulsion is suitable to prepare nanosized particles because the reaction is performed in the nanosized area. Emulsion synthesis method relays strongly on the type and concentration of surfactant used in the reaction process [76]. For example, the formation of micelles and vesicles stabilized with surfactants relies on the chemical structure of the surfactant, particularly, its molecular weight and size dimension. These micelles and vesicles provide a capable atmosphere for controlling the growth of nanoparticles. The organic layer can subsequently be removed by calcination, and the resultant product may give rise to a negligible change in crystal growth and particle sizes [75–77].

10.2.6 Template Method

In recent years, except in the conventional techniques, some innovative strategies, such as the template method and gel-casting technique, also developed to meet different kinds of practical needs. Kamieniak et al. [78] prepared a mesoporous HAP by a novel template method using carbon nanorods as a hard template. It is worth mentioning that this work first regarded carbon nanorods as a template to synthesize mesoporous HAP. The result showed that this method can successfully synthesize single phase HAP with the specific surface area of $242.20 \pm 2.27\,m^2/g$ and average pore diameter of 3.5 to 18.9 nm. Ramay and Zhang [79] employed a new strategy combining the gel-casting and polymer-sponge methods to prepare microporous HAP scaffolds. The novel technique provided a well control over the microscopic morphology of scaffolds and improved their mechanical property. The resultant scaffolds have an exoteric, homogenous, and interconnected porous structure as well as a pore diameter distribution of 200–400 μm.

10.2.7 Synergistic Synthesis Methods

In order to obtain the HAP with better properties, crystalline degree, and morphology, the synergistic strategy characterized by the combination of two or more methods was preferred [80,81].

Among these attempts, hydrothermal-mechanochemical [82–85], hydrothermal-hydrolysis [86–89], and hydrothermal-microemulsion are regarded as the main methods, which have received wide attentions over the past decades. Banerjee et al. [90] developed a fluorescent erbium doped HAP (eHAP)-chitosan nanocomposite film. The nanosize eHAP was synthesized by a hydrothermal-assisted precipitation method using erbium (III) ions as dopant. Physicochemical characterization analysis demonstrated a combination and uniform distribution of eHAP in the CS film. Simultaneously, the strong antimicrobial effect was found to aim at *E. coli* and *S. aureus* for the as-prepared nanocomposite film. In addition, the doped film exhibited a well biodegradation and mineralization capability after 2 weeks in simulated body fluid. Comparatively, the combination of the mechanochemical treatment and the hydrothermal process is the most promising method to synthesize HAP due to the simple process and relatively lower cost [91].

The usual reactants or raw materials for synthesis of HAP mainly include Ca and P source. Calcium compounds usually originate from calcium salts, e.g., calcium nitrate, calcium hydroxide, calcium oxide, calcium carbonate. Similarly, P source mainly origin from usual chemicals of phosphorus salts, e.g., phosphoric acid and phosphate. Recently, inexpensive biogenic sources, such as the egg shell, bovine, pig or fish bone, coral, bamboo, and some exoskeleton of marine organisms as well as biowastes with abundant calcium and/or phosphorus species resides, have been used as potential candidates to synthesize HAP [92–96]. Sivakumar et al. [97] used a simple method to convert the calcium carbonate frame of the corals from India to HAP grains. The precursors (corals) with the associated aragonite and calcite phases were heated at 900°C to remove the residual organics and impurities. After calcination, the carbonate phase in the coral was decomposed entirely. Subsequently, the precursors (corals) are converted to HAP product by a hydrothermal reaction via the addition of di-ammonium phosphate. It is surprising that the HAP prepared by this method was in the form of powder and almost did not contain impurities. Holmes et al. [98] prepared HAP by using sea coral calcite as the raw material. After testing 52 dogs, the obtained materials combined with bone tissue very well and was as hard as the native bone tissue. This result confirmed the potential applications of sea coral calcite for synthesis of HAP.

Like other nanoparticles, HAP nanomaterials would also agglomerate during the synthesis process, which greatly affected their physical and chemical properties. Therefore, researchers developed some effective methods for the management of agglomeration, e.g., traditional surfactant-assisted synthesis methods, micro emulsion synthesis method and addition of a variety of additives, and modifier

or chelating agents in the preparation process [9]. Mobasherpour et al. [99] prepared the HAP powder from calcium nitrate and diammonium hydrogen phosphate solution via a precipitation technique and subsequent heat treatment. Results demonstrated that the size of HAP particles gradually increased in the range of temperature from 100 to 1200°C, but the HAP with hexagonal-dipyramidal phase was not transformed into other calcium phosphates up to 1200°C.

In order to avoid aggregation of nanoparticles, Hu et al. [100] immobilized the HAP on the surface of polymer matter (chitosan). In this process, a lucid and faint yellow chitosan (CS)/HAP nanocomposite was synthesized by a new and easy in situ hybridization method. The results of characterization analysis indicated that HAP nanoparticles were dispersed well in CS material, and this novel technique can be a friendly candidate to cope with the agglomeration problem of HAP nanoparticles.

For the synthesis of HAP, phase impurity is also a notable subject, especially for the eye-catching wet methods. In general, the impurity in HAP product is mainly calcium phosphate compounds, including monocalcium phosphate monohydrate, monocalium phosphate anhydrous, dicalcium phosphate dihydrate (brushite), octacalium phosphate, amorphous calcium phosphate, etc. It is worth noting that these impurities mostly originated from the high-temperature calcination process and the insufficient ripening for HAP, so that reducing the calcination temperature and prolonging the aging time are significant [40]. Koutsopoulos [101] employed and contrasted with three wet methods to prepare HAP and found that aging and precipitation kinetics are significant influence factors for the phase purity and crystalline structure of the HAP product.

Typically, a lot of factors (i.e., pH of reaction system, reaction temperature, the reactant proportion (Ca/P ratio), and post-treatment ways) may affect the synthesis process and the structure and property of HAP. Boskey et al. [102] studied the effect of temperature and pH of reaction solution on the formation rate of HAP from calcium phosphate. The level of reaction was detected through the percentage of crystallinity using X-ray diffraction analysis. It was found that the transformation kinetics is accordant with pseudo-first-order kinetic model, and only dependent on the pH of reaction solution at a constant temperature. In addition, a solution autocatalytic mechanism is proposed to explain the metastability of the amorphous product.

The mechanism or formation process of HAP is different for different kinds of methods. However, these synthesis methods generally include two processes: nucleation and crystalline growth. The specific details or formation mechanism of HAP are distinct for different methods. For dry methods, the nucleation takes place in a hydropenic environment; but in a moist atmosphere for wet methods. However,

in order to develop a HAP with uniform morphology and structure, the post-calcination treatment is always necessary. Hunter et al. [103] studied the effects of nucleators or inhibitors on the certain proteins of mineralized tissues during the formation process of HAP. They studied the HAP-nucleating and HAP-inhibiting characteristic of proteins originating from bone [osteocalcin (OC), osteopontin (OPN), osteonectin (ON) and bone sialoprotein (BSP)], dentine [phosphophoryn (DPP)], and sintered cartilage [chondrocalcin (CC)]. It was shown that BSP and DPP possessed nucleation activity at the minimum concentrations of 0.3 μg/mL (9 nM) and 10 μg/mL (67 nM), respectively. OC, OPN, ON, and CC all cannot exhibit nucleation activity at the concentrations up to 100 μg/mL. Simultaneously, OPN was found to be an effective inhibitor for HAP formation [IC_{50} = 0.32 μg/mL (0.01 μM)], and OC was low potency [IC_{50} = 6.1 μg/mL (1.1 μM)]. In addition, BSP, ON, and CC all cannot show the inhibitory activity at the concentrations up to 10 μg/mL. These discoveries identified with the viewpoint that BSP and DPP may play roles in the initiation of mineralization in bone and dentine, respectively.

10.3 Applications of Hydroxyapatite

10.3.1 Drug-Delivery Carrier

Drug-delivery system (DDS) has received more attention because it may improve the delivery efficiency of drugs and achieve the controllable release of drugs. Drug-delivery carriers are the key to decide the performance of DDS. Usually, drug-delivery carriers should have a high surface area and good biocompatibility [104]. HAP, as a potential drug-delivery carrier, has recently attracted considerable attention because of its biocompatible, osteoconductive, and noninflammatory properties [105,106]. Researchers have used HAP nanoparticles to deliver various genes, proteins, and drugs [107,108]. In addition, the surface of HAP is rough, which favors the use of HAP in biomedical fields. The rough surface together with the “P” and “C” sites of HAP facilitates it to binding protein during the mineralization process [109]. Many approaches have been developed for the conjugation of therapeutic agents or targeting ligands on the surface of nanoparticles (Fig. 10.3). They can be classified in two major groups: one is the conjugation of drugs by means of cleavable covalent linkages, and another is attachment through physical interactions [110]. The use of HAP nanorods/nanoparticles as a drug-delivery carrier for delivering various proteins (growth factors) and drugs has been studied. Yang et al. [111] reported the synthesis of HAP nanoparticles with a hollow core and a mesoporous shell (hmHANPs). The synthesized hmHANPs exhibit superior drug-loading capacity and enhanced drug-release efficiency

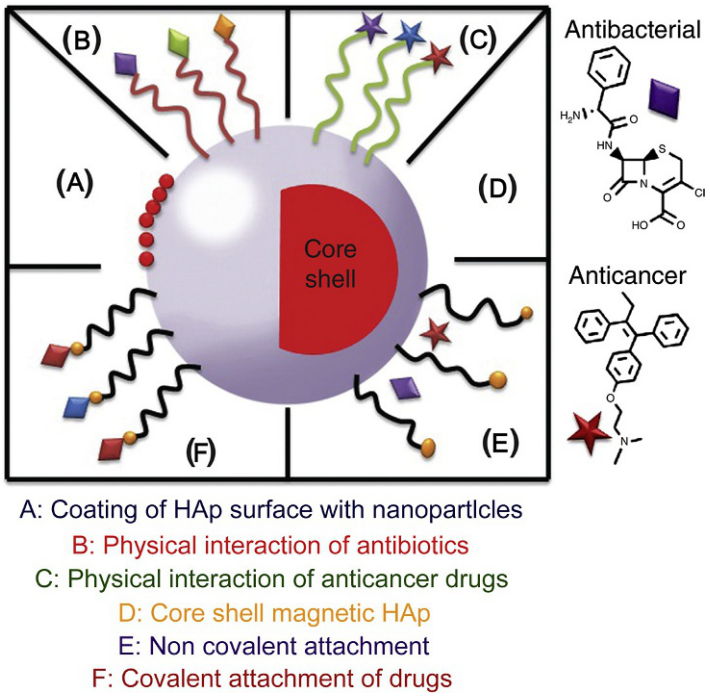

Fig. 10.3 Schematic presentation of drug-conjugation processes over HAP nanoparticles. Reproduced with permission from S. Mondal, S.V. Dorozhkin, U. Pal, Recent progress on fabrication and drug delivery applications of nanostructured hydroxyapatite, Wiley Interdiscip. Rev. Nanomed. Nanobiotechnol. 10 (4) (2018) e1504.

in comparison with the HAP nanoparticles without hollow structure. Therapeutic anticancer drugs can be loaded efficiently onto the synthesized hollow mesoporous hydroxyapatite nanoparticles (hmHANPs) and can be released through acid-assisted diffusion/dissolution controlled kinetics. Mesoporous HAP nanoparticles were successfully prepared using F127 as a template coupled with CTAB as a co-template by the hydrothermal method. The results of this research demonstrated the successful uptake and release of the model drug CAR in an amorphous state with a drug loading efficiency up to 24.87% [112]. Yang et al. [113] proposed the one-step synthesis of novel luminescence functionalized mesoporous HAP materials by doping Eu^{3+} during the synthesis of mesoporous HAP, resulting in the formation of multifunctional material. In addition, Son et al. [114] successfully developed a functional porous HAP scaffold containing 3D-localized drug delivery structures (polymeric microspheres). As an excellent drug-delivery platform for bone regeneration, dexamethasone (DEX) as a model bioactive molecule was efficiently added to the microsphere-containing porous HAP scaffold without biological malfunctions, and the release kinetics of DEX could be efficiently tuned through microsphere-capture technology. The spherical porous HAP microparticles (SP-HAP) as an injectable carrier for drugs such as IFNα, TE, and CyA were

studied [115]. These drugs could be injected with a small-bore needle (27 gauge), which reduced pain on injection. In addition, SP-HAP is biodegradable after subcutaneous injection and can provide a sustained release of bioactive proteins and lipophilic drugs. The PM/HA/CS-based oral drug delivery system was developed to enhance the solubility and oral bioavailability of poorly soluble drugs, and it was suggested that a PM/HA/CS-based drug delivery system is a promising strategy to combine the unique properties of three-dimensional macroporous HAP/CS foam and polymer micelles, which will enhance the solubility and oral bioavailability of poorly soluble compounds [116].

Smart SiO_2-based drug-delivery vehicles with high drug-loading ability, multi-responsiveness, and excellent biodegradability have been studied intensively. The novel nanoscale hybrid drug carrier with AuNR core and SiO_2/HAP shell (Au/SiO_2/HAP) was prepared and used for multi-responsive drug delivery (Fig. 10.4). AuNRs coated by SiO_2/HAP were obtained through base-catalyzed hydrolysis of tetraethyl orthosilicate (TEOS) and HAP was in situ formed via the reaction between calcium salt and phosphate. The introduction of HAP altered the mesoporous constitution of the original silica shell, resulting in the relatively higher drug-loading capability of Au/SiO_2/HAP nanoparticles. The Au/SiO_2/HAP nanoparticles exhibited distinguished NIR- and pH-responsive behavior and release behavior of Doxorubicin hydrochloride (DOX) drug [117]. The effective functionalization process of mesoporous silica SBA-16/HAP-based composite was achieved using a one-pot process by post-synthesis grafting [118]. The silica/HAP composite presented excellent biocompatibility, bioactivity, low susceptibility to immune response, and resistance to lipases and bile salts. These studies provided a facile route to fabricate

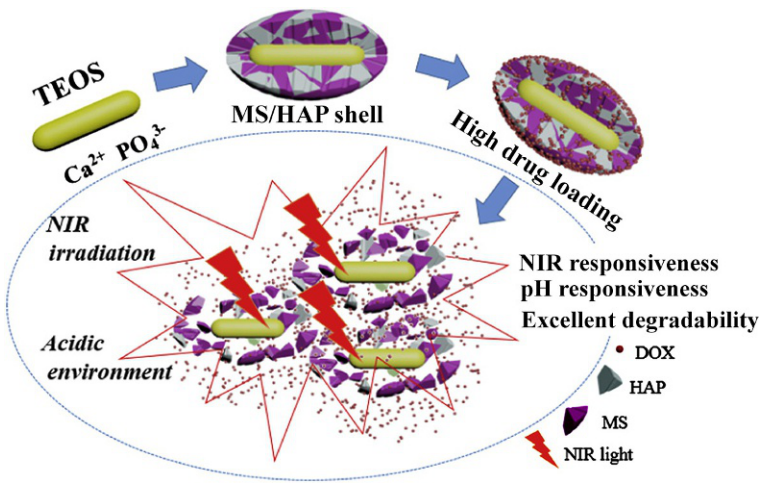

Fig. 10.4 Preparation and properties of Au/SiO_2/HAP nanoparticles. Reproduced with permission from Z. Song, Y. Liu, J. Shi, T. Ma, Z. Zhang, H. Ma, S. Cao, Hydroxyapatite/mesoporous silica coated gold nanorods with improved degradability as a multi-responsive drug delivery platform, Mater. Sci. Eng. C. 83 (2018) 90–98.

an efficient, safe, and smart HAP-based drug-delivery carrier, which lays a solid foundation to extend the application of HAP as a drug-delivery system.

10.3.2 Tissue Engineering

Bone is a natural organic-inorganic ceramic composite consisting of collagen fibrils containing embedded, well-arrayed, nanocrystalline, rod-like inorganic materials 25–50 nm in length [119,120]. But there is a growing demand for bone regeneration material due to various clinical bone diseases, such as bone infections, bone tumors, and bone loss by trauma [121]. Calcium phosphate is present in bones in the form of HAP crystals, which provides rigidity to the bone. The HAP components are similar to those of bone, and the length and width of HAP crystals in bone are in the nanometer range. The presence of HAP in an implant not only enhances the osteoinductive behavior of the implant, but also improves the osteoconductive properties between the implant and the bone cells [122]. HAP has been frequently used for bone tissue engineering, including bone repair and bone augmentation, as well as coating implants or acting as fillers in bone or teeth [123–126].

HAP-based artificial bones are now widely used in clinical practice and show satisfying repair function in a series of studies [127,128]. Zhou et al. [129] reported the clinical evaluation of SB-1 as a synthetic bone in sinus bone grafting. The used SB-1 consists of synthetic HAP with the particle size of 500–1400 μm, and it has the same chemical composition as the inorganic part of human bones. The result showed that the SB-1 was well integrated with the surrounding host bone and promoted induction of new bone, leading to bonding with newly formed bone and tge recovery of damaged bone tissue. Zhu et al. [130] evaluated the osteoconductive properties of nano-HAP material and its potential application as artificial bone in repairing bone defects. The authors attempted to analyze the scientific basis of these properties, and they proved that the nano-HAP artificial bone can potentially be used for bone defect treatment. The features of smaller HAP nanoparticles may more closely resemble features of HAP during biomineralization than features of the larger HAP particles that are conventionally used [131]. Nano-HAP may promote osteoblast adhesion, proliferation and synthesis of alkaline phosphatase, and lead to rapid repair of hard tissue injury [132].

HAP ceramics have been widely used as substitutes of artificial bone because of their high biocompatibility, bioaffinity, and osteoconductibility. However, due to the closed structure, the conventional porous HAP has non-uniform pore geometry and low interpore connections, so it is very difficult to completely fill the implant pores with

newly formed host bone [133]. Porous HAP ceramics with highly interconnecting structures have been developed, and osteoconduction can occur deep inside such ceramics. Tamai et al. [134] developed fully opened interconnected porous HAP ceramics (IP-CHA: porosity, 75%; average pore size, 150 μm; and average interpore connections, 40 μm) by adopting a "foam-gel" technique, which showed well-organized interconnective porous structure and superior osteoconductivity in vivo. Ahn et al. [135] suggested that the HAP-based Zr bioceramic materials with a fine structure and enhanced mechanical properties could be used both in dental and orthopedic implanting materials. However, there are some weaknesses, such as weak intensity, brittleness and fatigue failure, and slow degradation; therefore, the applications of nHAP ceramics as clinical materials are limited [136]. To strengthen HAP, researchers have carried out omnidirectional investigations, but the development of HAP with good biological properties matched with good mechanical properties is still challenging [137]. Since the synthesized HAP is very brittle, the implant materials composed of hard and soft phases (composite materials) are used for total bone replacement.

Chitosan (CS) has been proven to be excellent in bone tissue engineering owing to its excellent pore-forming ability, binding capacity with anionic molecules, antibacterial activity, and biodegradation [138]. The addition of nHAP in CS can increase the mechanical properties of nanocomposites, which mimic the natural structure of bone. Several methods have been applied in the preparation of nHAP-chitosan nanocomposites [139]. A two-step approach that combines an in situ co-precipitation synthesis route with electrospinning process has been employed to prepare new types of hydroxyaptite/chitosan (HAP/CTS) biomimetic nanocomposite nanofibers [140]. Results showed that the HAP- incorporated nanofibrous scaffolds appear to have significantly improved bone forming ability as compared to CTS alone scaffolds. The nHAP-chitosan-carboxymethyl cellulose composite scaffold with 30 wt% of carboxymethyl cellulose was prepared by a freeze-drying method, which showed the most ideal porous structure with the pore size ranging from 100 to 500 μm; porosity of 77.8%; and the highest compressive strength of 3.54 MPa [141]. Liu et al. [142] has prepared HAP/CS nanofibers by combining an in situ co-precipitation approach with an electro-spinning process. It was found that the nHAP/CS scaffolds may promote bone regeneration by supporting adhesion, proliferation and activating integrin-BMP/Smad signaling pathway of mBMSCs both in vitro and in vivo. Recently, Maji et al. [143] demonstrated the applicability of nHAp based gelatin (G)—carboxymethyl chitosan (C) macroporous scaffold for bone tissue engineering application. The results revealed that the scaffolds had multi-modal pore-size distribution with large pore size and high water-uptake capacity. The SGC scaffold degrades in a sustained way in the presence of the enzymea lysozyme

and collagenase. The mechanical strength of the scaffold was found to be higher than non-macroporous scaffold with an even distribution of HAP throughout the scaffold.

Sodium alginate (SA), the natural polysaccharide derived from brown sea algae, is believed to be a promising material with good scaffold-forming ability that can be used to treat the loss or failure of organs [144]. Pure SA shows some deficiencies, such as lack of cellular interactions and weak mechanical strength, which may limit its applications in tissue engineering. The porous gHAP/SA nanocomposite scaffolds have been prepared successfully by using a facile solution mixture and a freeze-drying method. The gHAP/SA scaffolds exhibit a highly porous structure with porosities of over 85% and average pore sizes ranging from 156 to 190 μm, depending on the content of gHAP. It was found that the incorporation of gHAP nanoplates in the SA matrix not only improves the compressive strength, modulus, and thermal stability of neat SA, but also promotes the proliferation of MG-63 cells [145]. The 3-D porous nanocomposite scaffold of g-HAP containing RGD-conjugated copolymer has been fabricated and tested for repairing rabbit bone defects using tissue-engineering technology. The g-HAP/PLGA(HP), RGD-copolymer/g-HAP/PLGA(RHP) and BMP-2/RGD-copolymer/g-HAP/PLGA (BRHP) scaffolds were evaluated in the critical-sized defects of radial bone of rabbit for bone-tissue regeneration. The combined RGD-copolymer with BMP-2 exhibited the best bone-healing quality, as shown in Fig. 10.5 [146].

In addition, a variety of ideal scaffold materials have been fabricated and evaluated, such as HA/PU [147], HAP/PVA [148], HAP/PA [149], and others [150,151]. In general, polymers and ceramics can all be used as scaffolds for tissue-engineering applications. Polymers offer the advantages, such as ease of processing by various methods, good biocompatibility, and degradation rate, but fail to obtain the desired mechanical properties. Ceramics may show good biocompatibility, but they are fairly brittle and somewhat difficult to process. Despite the recent advances, there is a necessity for more research to prepare an infection-free implanting material with sufficient mechanical strength.

10.3.3 Antibacterial Materials

HAP itself has limited antibacterial performance [152]; even worse, HAP is very hydrophilic, and bacteria are very easy to adhere and enrich on its surface [153,154], which induced bacterial infection during the use of HAP-based materials [155] and limited its application in biological materials. How to avoid the bacterial infection of HAP-based biomaterials is of great clinical significance and is one of the hot issues that concern researchers. In order to improve the antibacterial

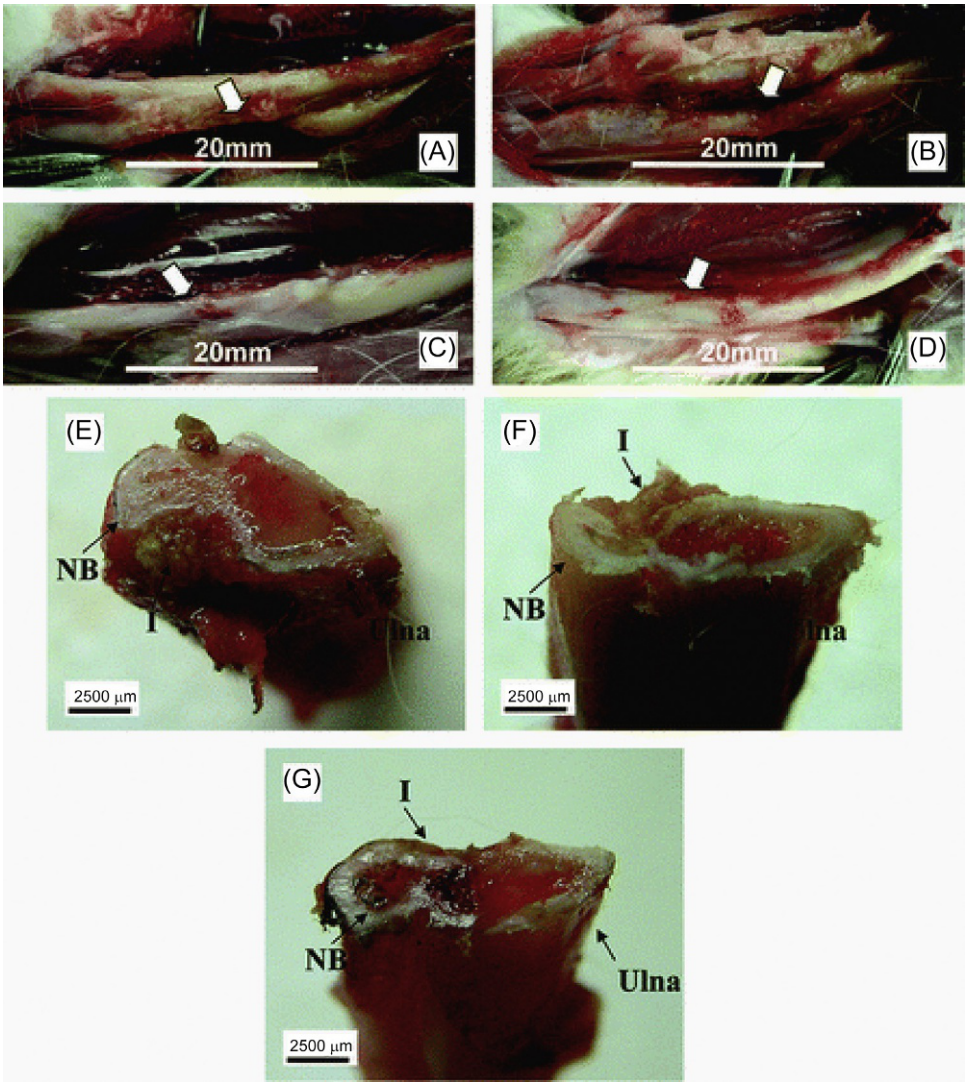

Fig. 10.5 Macroscopic observation of the representative repaired tissues at the critical-sized defects of rabbit radius in untreated control (A) and implanted with tissue-engineered porous scaffolds of HP (B, E), RHP (C, F), and BRHP (D, G). The *bold arrows* indicate the areas of radius defect or repaired tissues. (E–G) cross sections at the center of the repaired tissues, and the letters of I and NB indicate the implants and the newly formed bones of radius, respectively. The pictures were taken by a digital camera. Scale bars are 20 mm (A–D) and 2500 μm (E–G). Reproduced with permission from P. Zhang, H. Wu, H. Wu, Z. Lù, C. Deng, Z. Hong, X. Jing, X. Chen, RGD-conjugated copolymer incorporated into composite of poly (lactide-co-glycotide) and poly (l-lactide)-grafted nanohydroxyapatite for bone tissue engineering, Biomacromolecules 12 (7) (2011) 2667–2680.

properties of the HAP-based biomaterial, it is generally possible to add a certain antibacterial substance/agent so that the HAP-based biomaterial has the ability to inhibit or kill microorganisms attached on its own surface or an adjacent surface. Here, we briefly summarize the latest research progress on HAP antimicrobial biomaterials.

10.3.3.1 Doping Ions as an Antibacterial Material Additive

The incorporation of trace elements into the crystal structure of HAP is an effective strategy to prepare HAP antibacterial materials. It has been verified that the introduction of Ag [156–161], Zn [162–165], Cu [166–169], or F [170–173] can increase the antibacterial activity of HAP. In addition, the introduction of these elements can improve the physical, chemical properties, and biocompatibility of HAP, as well as the applicability of HAP in the biological field.

Silver (Ag) ion is the most commonly used metal antibacterial agent with good thermal stability, biocompatibility, and low cytotoxicity [174]. Ag^+ doped HAP has been synthesized by various methods, such as the co-precipitation method [152], microwave-reflux method [175], sol-gel method [176,177], ultrasonic-precipitation method [178], electrostatic spray-pyrolysis method [179]. Ag doping can enhance the antibacterial activity of HAP biomaterials. Riaz et al. [180] employed an inexpensive and conventional precipitation method to optimize the concentration of doped silver to synthesize HAP $Ca_{10-x}Ag_x(PO_4)_6(OH)_2$ (x = 0, 0.1, 0.3, 0.5, 0.7 M), and calcined at 900°C to obtain single-phase HAP. It was found that Ag^+ replaced the Ca^{2+} site in the crystal lattice, and the lattice parameters *a* and *c* change with the increase of the silver concentration. The results of in vitro bioactivity and antibacterial experiments showed that all silver-doped HAP maintains biological activity and significantly increased the antibacterial activity against *Staphylococcus aureus*, and the antibacterial ability is significantly enhanced with the increase of Ag^+ doping concentration. Qi et al. [181] synthesized a bioactive HAP nanobelt with antibacterial properties by using the hydrothermal uniform precipitation method for synthesizing Ag-doped HAP (Ag_xHAP) [$Ca_{10-x}Ag_x(PO_4)_6(OH)_2$] (x = 0, 0.2, 0.5). Authors systematically evaluated their antibacterial properties against *E. coli* bacteria and the cytotoxicity against Swiss embryonic mouse fibroblasts (3T3-J2) cells. Their work showed that the incorporation of moderate amounts of Ag into the HAP nanobelts increased its antibacterial properties and biological activity, and the HAP nanobelts also showed enhanced mechanical properties and good flexibility.

Zinc (Zn) is an important trace element in the human body. It can stimulate the synthesis of osteoblast protein to stimulate bone formation [182]. Zn is also a commonly used antibacterial agent with low costs and good biocompatibility [183,184]. Incorporation of Zn^{2+} not only endows HAP with antibacterial activity, but also increases

its biological activity. Sergi et al. [185] prepared a Zn-doped HAP (HAP + Zn) coating on a Ti6Al4V substrate by a solution precursor plasma spray (SPPS) process, and investigated the microstructure, bioactivity, cytotoxicity, and antibacterial properties of the coating. The results showed that SAOS-2 osteoblast-like cells adhered well and proliferated on Zn-doped HAP coatings, with no cytotoxicity to human osteoblast Saos-2 cells. The coating showed moderate antibacterial efficacy against *Escherichia coli*, and significant effectiveness for *Staphylococcus aureus*. Wang et al. [186] prepared Sr-doped, Zn-doped, and Sr/Zn-co-doped porous HAP scaffolds by combining an ion-exchange method and a foaming method. The density functional theory (DFT) and experimental results showed that Sr/Zn is doped into HAP, and lattice parameters *a* and *c* increased in Sr-doped HAP; *a* and *c* decreased in Zn-doped HAP. The Sr/Zn co-doped HAP scaffold promoted BMSC differentiation, showed good osteoinductivity, and had significant inhibitory effect on *Staphylococcus epidermidis*.

Copper (Cu) can also prevent and inhibit bacteria and is also an essential micronutrient essential for the immune system and oxidoreductase [187]. Hidalgo-Robatto et al. [167] used pulsed laser deposition (PLD) to prepare Cu-HAP and Zn-HAP coatings with two different metal ions. The extensive physicochemical characterization showed that Cu^{2+} and Zn^{2+} ions were successfully doped into HAP. The antibacterial properties of Cu-HAP and Zn-HAP coatings were observed, and they all exhibited antibacterial activity against *Staphylococcus aureus* and *Escherichia coli*. Shi et al. [166] used inositol hexakisphosphate (IP6) as regulator of crystal morphologies to synthesize micro/nanostructures and Cu^{2+}-doped HAP (HAP-IP6-Cu) microspheres under hydrothermal conditions. The effects of microstructure and chemical composition on the bioactivity of the materials were investigated, and the synergistic effects of micro/nano hybrid structures and Cu^{2+} on cell behavior were evaluated. The results showed that HAP-IP6-Cu can promote cell proliferation and osteogenic differentiation, and effectively inhibit *Staphylococcus aureus* and *Escherichia coli*, suggesting an excellent cytocompatibility and antibacterial property.

Fluoride (F) is also a common antibacterial agent. F has excellent osteogenic activity and is an essential element in bone and tooth tissues, promoting mineralization and directly participating in the bone formation process [188]. F doping is beneficial to increase the antibacterial ability and biological activity of HAP-based biomaterials. Naske et al. [172] synthesized pure HAP (HAP) and HAP nanopowder (FHAP) with different substitution amounts of fluorine by a hydrothermal method. The effect of fluorine concentration on the crystallite size, crystallinity, and morphology of the synthesized powder was studied. It was found that with the increase of fluorine substitution, the crystallinity of HAP powder increased gradually; the cell

volume decreased, and >50% substitution led to the appearance of CaF_2 phase. FHAP has antibacterial activity against *Gram-negative* (*E. coli*) *and Gram-positive* (*S. aureus*) *strains* and is not cytotoxic, but powder with 50% or more fluorine substitution is not conducive to the proliferation of osteoblasts. Wang et al. [189] synthesized a series of fluorine-substituted calcium-deficient HAP with a FHA molar ratio (mol F^-/mol apatite) of 0.002–0.2. The sample with a molar ratio of 0.02 (F0.02) has excellent osteogenic activity and high antibacterial ability. This can be explained by the unique microstructure of the F0.02 sample. Calcium deficiency in F0.02 has a layered structure with a negative Zeta potential. It also shows abundant Ca(II) vacancies and lattice defects, leading to the formation of a net dipole moment, a change in the level of potential energy, and a strong acid site in the necessary bioactive center.

10.3.3.2 Antibiotics-Loaded Antibacterial Material

HAP loaded with antibiotics can also improve the antibacterial properties of HAP-based biomaterials by controlling the release of antibiotics [190–196]. Li et al. [195] reported a technical route to prepare HAP-gentamicin sulfate (GS) composite coating by a vacuum cold spray (VCS) at room temperature to construct an antibiotic-loaded coating for local delivery of gentamicin. The release kinetics, antibacterial properties, and biocompatibility of gentamicin were systematically studied in vitro. The results show that HAP-GS can effectively load antibiotic coatings, and the coating has long-term antibacterial ability. Ramírez-Agudelo et al. [196] encapsulated doxycycline (Dox) and HAP nanoparticles (nHAP) into poly-ε-caprolactone/gel (PCL-Gel) solutions with various ratios and prepared Dox/nHAP-loaded PCL-Gel composite nanofibers (Dox/nHAP/PCL-Gel) by using electrospinning technology. Dox/nHAP/PCL-Gel nanofibers can release Dox in vitro, giving them antibacterial activity against *Gram-positive Staphylococcus aureus* (*S. aureus*) and *Gram-negative Porphyromonas gingivalis* (*P. gingivalis*). In addition, Dox/nHAP/PCL-Gel also can be used for the treatment of tumors.

10.3.3.3 Composite Antibacterial Agent

The addition of natural antibacterial agents such as alginate [197], CS [198], or the combination of natural antibacterial agents, inorganic antibacterial agents, and other active antibacterial substances [199–203] to form HAP-based biomaterials with improved antibacterial properties has also been studied widely. Ohtsu et al. [204] studied the antibacterial effect of the zinc oxide/HAP coating that is prepared by chemical solution deposition followed by a heating process. The amount of ZnO precipitates was controlled by changing the

concentration of ZnO in the deposition solution, and thereby the release rate of surface Zn was also controlled. The ZnO/HAP coating exhibits excellent antibacterial efficacy against *Escherichia coli* and *S. epidermidis* due to the contact killing effect of ZnO. Sivaraj and Vijayalakshmi [205] studied the synthesis of bioactive HAP/multi-walled carbon nanotube (HAP/f-MWCNT) composite coatings on 316L SS implants by a spray pyrolysis method. The results show that the crystallinity of HAP decreases after the addition of f-MWCNT, and the morphology appears as a multi-space nanosphere with reduced particle size. The mixed HAP/f-MWCNT nanocomposite coating greatly enhanced cell adhesion and differentiation, showing enhanced antibacterial activity, with the inhibition zone of 12 mm for *Escherichia coli*. The alginate/HAP (SA/HAP) bio-nanocomposite membranes reinforced by HAP nanoparticles (HAP NPs) were prepared by incorporating different concentrations of HAP NPs (1%, 3% and 5%) into the alginate solution [197]. The SA films incorporated with different concentrations of HAP NPs reasonably reduced gram-positive bacterium L. *monocytogenes* population growth with respect to control film. The hybird coating (Lys/CS/Ag/HAP) of lysozyme (Lys), CS, silver (Ag), and HAP on the Ti surface proved to be favorable for cell adhesion and proliferation, and the antibacterial effect of Lys/CS/Ag/HAP mixed coating on *Escherichia coli* and *Staphylococcus aureus* was over 95.28% and 98.02% within 12hs, and after 5 days, reaching 95.42% and 97.46%, and almost no cytotoxicity [206]. The polydopamine (PDA)-assisted HAP and lactoferrin multilayer structures on the surface of Ti substrates showed improved proliferation and differentiation, which can reduce the activity of bacteria (*Escherichia coli* and *S. epidermidis*) and has a short-term antibacterial adhesion [207].

10.3.4 Catalysis

HAP and HAP-based composites can be synthesized by a simple method and have been potentially used in the field of catalysis due to their obvious catalytic effects and good cycle stability. There are a lot of reports about the applications of HAP-based catalysts in cross-coupling reactions [208,209], condensation reactions [210,211], oxidation reactions [212,213], photocatalytic reactions [214,215], and other miscellaneous reactions [216,217]. In this regard, Fihri et al. [218] made a detailed review on the synthesis, structure, and applications of HAP in heterogeneous catalysis.

From the perspective of materials' science, HAP as a catalyst and catalyst carrier has the following advantages [219]: (i) Strong ion exchange capacity: the ions in HAP can exchange with other ions and can be used to prepare a catalyst with loading of various metals, metal oxides, or homogeneous complexes; (ii) Adjustable surface acidity

and alkalinity: the surface acidity and alkalinity of HAP can be adjusted by changing the ratio of calcium to phosphorus in the preparation process of HAP to meet the needs of different catalytic reactions; (iii) Easy surface modification: hydroxyl groups is rich on the surface of HAP, which can be modified by various organic compounds with polar functional groups. All these provide a superiority of HAP for fabricating diverse of HAP-based catalysts.

10.3.4.1 HAP-Supported Metal Catalyst

HAP-supported metal or metal-oxide catalysts are commonly used in various reactions, such as alkane oxidation/dehydrogenation, alcohol oxidation/dehydrogenation, epoxidation of olefins and aldehydes and ketones, oxidation of amines or aldehydes. Othmani et al. [220] synthesized calcium-copper HAP nanocrystals (CuHAP) with a maximum Cu content of about 15 at.% by a co-precipitation method. The substitution of Cu for Ca results in a decrease in the lattice parameter of HAP. As the Cu content increases, the crystallinity, crystal size, and thermal stability of CuHAP decreases, but the surface area increases. The effect of Cu content on the catalytic activity of CuHAP for degradation of organic dyes was also studied, and the finding was that CuHAP nanomaterials have high activity (70%) for the discoloration of naphthol blue black solution. The Cu functionalized HAP catalyst was also prepared by Schiavoni et al. [221] and used for NH_3-SCR reaction. Similarly, the HAP-supported Co and Co–Ce catalysts were prepared by incipient wetness impregnation and were applied to steam reforming of glycerol reaction to evaluate the catalytic performance of Co and Co–Ce catalysts [222], which exhibit high-glycerol conversion efficiency and selectivity to hydrogen. In addition, the addition of Ce also improved the H_2 selectivity and glycerol conversion and improved its stability because Ce inhibits the growth of cobalt particles and the strong interaction between Co and Ce in the catalyst. The Ni^{2+} and Co^{2+}-exchanged HAP by the conventional impregnation method and produced new Ni-Co-HAP bimetal particles with high catalytic activity, excellent selectivity, and good catalytic stability during the dry reforming methane (DRM) process. High catalytic performance is obtained at 700–750°C; the conversion of CH_4 and CO_2 is up to 73% and 79% at 750°C. CO and H_2 are the main products of the reaction, and the selectivity reaches about 80%–90%. Catalytic activity stabilized to 50 or 160 hs of reaction [223]. The HAP coatings loaded with catalytically active Pd nanoparticles with controllable size and size distribution were synthesized by a multi-stage electrochemical method, which showed significantly higher catalytic activity in the model dye reduction reaction than commercial Pd nanoparticle samples [224]. Zhang et al. [225] synthesized a dense and thermally stable Y^{3+} and F^- co-doped HAP film with large internal polarization and used it as a carrier for

supported TiO_2 to improve the photocatalytic performance of TiO_2. It is found that the photocatalytic efficiency of TiO_2 nanoparticles on polarized HAP supports is much higher than that of TiO_2 nanoparticles on depolarized HAP supports. The internal polarization of the HAP carrier promotes the separation of photogenerated electrons and holes in the TiO_2 nanoparticles, thus mitigating the recombination of charge carriers. In order to meet the requirements of different catalytic reactions and applications, different types of metal or metal-oxide supported HAP catalysts have been developed, such as Pd and Ni-doped HAP catalysts for catalytic reaction of methane oxidation [226], Rh(x)/HAP (x = 0.5, 1 and 2 wt%) catalysts for partial oxidation of (POM) and steam reforming (SRM) of methane [227], Au nanoparticles (AuNP)/HAP nanowires catalytic paper for continuous flow catalytic reduction of 4-nitrophenol and an organic dye [228].

10.3.4.2 HAP-Acid-Base Catalyst

The stoichiometric form of HAP is $Ca_{10}(PO_4)_6(OH)_2$ with a Ca/P molar ratio of 1.67. In fact, the radius of ions in HAP allows for considerable ion transfer or loss within its crystal structure, so that HAP is a non-stoichiometric calcium phosphate compound with a Ca/P ratio of 1.50–1.67. Therefore, when HAP was used as a catalyst, it contains both an acidic site and a basic site. It is known that highly crystalline HAP at a Ca/P ratio of 1.50 acts as an acid catalyst, while it acts as a basic catalyst at a Ca/P ratio of 1.67. When the Ca/P ratio of HAP is between 1.50 and 1.67, HAP has the dual characteristics of acid catalyst and basic catalyst [229–231]. In addition to adjusting the Ca/P ratio, the substitution of related ions in HAP was usually used to regulate the acidity and alkalinity of HAP surface, such as vacancies or Sr^{2+}, Mg^{2+}, Na^+, and K^+, instead of Ca^{2+} ions; vacancies, F^-, Cl^-, CO_3^{2-}, etc. substituted OH^- anions; CO_3^{2-}, HPO_4^{2-}, VO_4^{3-}, etc. replace PO_4^{3-}anions [232]. The acid-basic sites of HAP can be used to catalyze the reactions of hydrolysis, alcoholysis, esterification, and esters. Tsuchida et al. [231] prepared HAP catalysts with different Ca/P molar ratios by controlling the pH of the solution during precipitation synthesis, and found that the distribution of the acidic sites and the basic sites on the surface of the catalyst changed as the Ca/P ratio of the HAP changed. The use of HAP catalysts facilitated the high selectivity for synthesis of valuable compounds from ethanol, and the selectivity of the product was strongly correlated with the acidity and basicity of the HAP catalyst. Ghantani et al. [233] synthesized a HAP catalyst having a Ca/P ratio ranging from 1.3–1.85 by coprecipitation, changing the pH of the calcium and phosphorus precursors, and it was used as a vapor phase dehydration of lactic acid to acrylic acid. It was found that HAP with Ca/P ratio of 1.3 showed higher catalytic efficiency, and the conversion of acrylic acid was 100%. The selectivity was 60% at 375 °C and 50% lactic acid concentration, which is related to an

increase in acidity and a decrease in alkalinity of the HAP catalyst. The Sr-HAP catalyst with a high Sr/P molar ratio (1.58–1.70) was synthesized under hydrothermal conditions, which has a relatively higher density of basic sites. The Sr/HAP catalyst exhibited higher catalytic activity and 1-butanol selectivity in ethanol-catalyzed conversion at 300°C [234]. The modified HAP (Na-HAP) catalyst with bifunctional acidity and basicity was prepared by impregnated HAP with $NaNO_3$, which effectively catalyzed the cross-aldol condensation of aromatic aldehydes and cyclic ketones in a microwave environment to obtain α-α′-(EE)-bis(benzylidene)-cycloalkanone [235]. The introduction of Cs into the structure of HAP produced a new Cs-doped HAP catalyst, which exhibits high selectivity for direct conversion of bio-lactic acid to 2,3-pentanedione (72.3%) due to synergistic catalysis between surface basic sites and acidic sites [236]. The design of porous HAP provides a new way to prepare high-efficiency catalysts. The nanoporous HAP, having an acid–base functional group, was synthesized using a P123 triblock copolymer as a structure directing agent by a simple hydrothermal method to control the Ca/P ratio, which exhibits excellent catalytic activity, high conversion, product selectivity and reusability, and achieves 100% solketal selectivity at 90% conversion of bioglycerol [237].

10.3.4.3 Other HAP Catalyst

Since HAP is surface-active, its surface activity can be changed by surface modification or by controlling the crystalline surface of HAP to enhance catalytic activity for certain reactions. Siavashi et al. [238] prepared sulfonated nano-HAP functionalized with 2-aminoethyl dihydrogen phosphate (HAP@$AEPH_2$-SO_3H) catalyst, which can catalyze the direct esterification of carboxylic acids and alcohols with high selectivity and high yield. In addition, the HAP@$AEPH_2$-SO_3H solid acid catalyst can also be used for rapid one-step synthesis of 4,4′-(arylmethylene)-*bis*-(3-methyl-1H-pyrazole-5-ol) compound [239]. Oh et al. [240] controlled the crystal orientation in the HAP-based catalyst film by adopting the seed hydrothermal growth method to achieve the facet *c*-surface (002) crystal-face exposure. The area activity of the HAP-based catalyst based on *c*-surface exposure was found to be 47 times higher in the methane oxidation reactions than the *a*-surface in the HAP-based catalyst due to the preferential formation of oxide ions and vacancies on the *c*-surface.

10.3.5 Reinforce Filler of Polymer Materials

Polymer/HAP nanocomposites are an outstanding example of nanostructured materials where synergy between the inorganic component and the polymer matrix represents the key to the amazing properties and derived applications of this class of composite

materials, which have been used in sensors, photocatalysts, antibacterial agents, and electronic and biomedical materials [241]. The importance of HAP in the bone-tissue engineering field has been reported extensively. In most polymer composites, HAP has been used as an enforcer to improve mechanical strength and bioactivity of the composite material. Zuo et al. [242] synthesized a HAP/polyamide/polyethylene composite and proved that the chemical adhesion and tight mechanical coupling between HAP and polyamide lead to improvement of mechanical properties of HAP-reinforced polyamide composites. Russias et al. [243] fabricated a HAP/PLA composite with the elastic modulus of 10 GPa and found that the distribution of ceramic particles in a polymer matrix makes it quite susceptible to environmental degradation. Dalby et al. [244] prepared a HAP/poly(methylmethacrylate) (PMMA) composite and revealed that this material acts as a substrate for human osteoblast-like cells. The homogeneous PLGA/g-CHAP nanocomposites were prepared by introducing the surface-modified CHAP nanoparticles [245]. The tensile strength, fracture strain, and tensile modulus increased after the addition of g-CHAP filler, indicating that g-CHAP particles have both reinforcing and toughening effects on the composites. Increasing g-CHAP contents in composites was advantageous to the cell adhesion and proliferation [245]. The HAP-based three-dimensional composite scaffolds with controlled microstructures and an interconnected porous structure, together with high porosity, were fabricated using an emulsion freezing/freeze-drying technique [246], gas foamed by a pressure-quench method [247], a simple mixing method [248], and the sol-gel method [249]. Fracture surfaces of PCL/HAP composites showed a well-dispersed and homogeneous distribution of HAP nanowires within the PCL matrix. Mechanical testing revealed that the Young's and compressive moduli of PCL/HAP composites increased from 193 to 665 MPa and from 230 to 487 MPa, respectively, after incorporation of 50 wt% HAP [250].

The combination of polysaccharides and HAP is also a new way to prepare biocompatible and safe nanocomposite materials. Banerjee et al. [90] developed luminescent chitosan-HAP nanocomposite films using erbium ion doped HAP as an inorganic component, which can be used as antimicrobial dressing material, fluorescent cell regeneration scaffold, or implant material. Fig. 10.6 shows the probable antimicrobial action mode of e-HAP doped CS film. The microbicidal attribute of CS is widely accepted and is generally realized by membrane disruption, loss of cellular proteins, and change in membrane permeability.

HAP was incorporated into CS/PVA matrices to form a kind of bioceramic-biopolymer nanocomposite. Since CS and HAP are bioactive and osteoconductive, the electrostatic co-spinning of CS/PVA and nanosize HAP can form potential nanofibrous osteoconductive

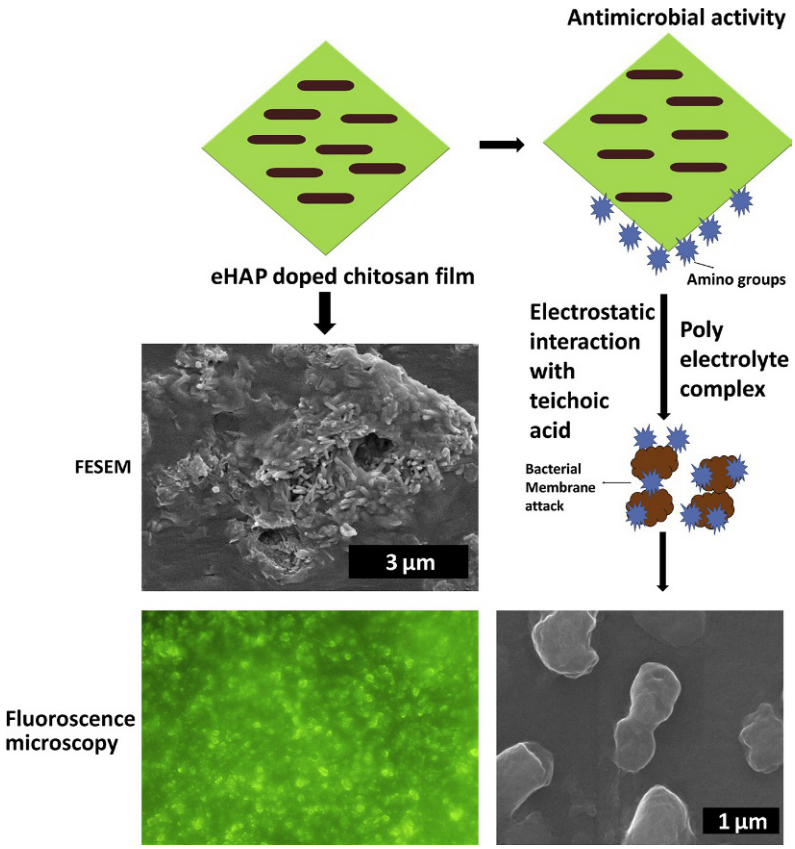

Fig. 10.6 Probable action mode of e-HAP doped CS film. Reproduced with permission from S. Banerjee, B. Bagchi, S. Bhandary, A. Kool, N.A. Hoque, P. Biswas, K. Pal, P. Thakur, K. Das, P. Karmakar, Antimicrobial and biocompatible fluorescent hydroxyapatite-chitosan nanocomposite films for biomedical applications, Colloids Surf. B: Biointerfaces 171 (2018) 300–307.

and bioactive nanocomposite scaffolds [251]. Katti et al. prepared the HAP-chitosan-montmorillonite nanocomposite with good biocompatibility by a precipitation method. This composite exhibited improved mechanical strength and better cell proliferation rate [252]. In addition, the CS/HAP composite nanofiber membrane was produced by an electrospinning process. The application of the prepared membrane for removal of lead, cobalt, and nickel ions from aqueous solution was investigated [253].

In addition to CS, other naturally abundant polymers like cellulose are also good candidates for the preparation of bio-nanocomposites. Bacterial cellulose possesses higher water-holding capacity, higher crystallinity, higher tensile strength, and a finer web-like network compared with other biodegradable polymers such as collagen, CS, chitin, and gelatin [254]. Wan et al. [255] synthesized porous HAP/bacterial cellulose nanocomposites with 3-D network structure by employing an electrospinning technique. The results suggest that the HAP/bacterial cellulose nanocomposites are promising for applications in tissue

engineering because of the biocompatibility of the materials and the bioactivity of HAP [256].

A variety of biocompatible nanocomposites based on collagen and HAP have been reported. For example, the HAP/collagen composite prepared by controlling the pH and temperature in the co-precipitation reaction process has characteristics similar to natural bone because it is able to induce the development of osteogenic cells and bone remodeling units [257]. The introduction of glutaraldehyde (GA) as a chemical cross-linker into HAP/collagen nanocomposite enhanced its mechanical strength by both inter- and intra-fibril cross-linkages among collagen fibrils in the composites [258], and the nanocomposite shows a bone-like structure through a self-organization mechanism under a biomimetic condition [259].

Gelatin is a translucent and solid substance derived from collagen from various animal by-products. Azami et al. [260] prepared a 3D nanocomposite scaffold of gelatin with HAP through a novel layer solvent casting combined freeze-drying technique. The scaffolds are of a well-defined interconnected porous structure with pore sizes ranging from 100 nm to 1 μm; the densities range from 75% to 93%; the compressive modulus of about 180 MPa and pore size range from 300 to 500 μm [261].

Silk fibroin (SF) has attracted great interest because of its outstanding biocompatibility, biodegradability, and minimal inflammatory reaction [262]. HAP/SF biocomposite was prepared by a freeze-drying technique [263]. The needle-like HAP crystals with the diameter of about 10 nm and the length of about 50–80 nm were observed to be distributed uniformly in the porous nHA/SF scaffolds.

10.3.6 Adsorption and Separation Materials

Adsorption and separation are very important application fields of HAP due to its porous structure, ion-exchange capability, and other available superiority. Recently, the adsorption of HAP for heavy metals, dyes, antibiotics, and other common organic or inorganic contaminates have been studied intensively. Xu et al. [264] studied the adsorption performance of HAP for Pb(II) from wastewater. It was found that the removal rate of Pb(II) is kinetically rapid. The Pb(II) concentration in solution reduced from 100 mg/L to <0.5 mg/L within several minutes, and the dissolution of HAP and the combination of lead apatites represent the main reaction mechanisms. The adsorption behavior of Sn^{2+} on nano HAP was studied, and it was determined that the adsorption process can be defined well by the Langmuir isotherm model with a maximum adsorption capacity of 2500 mg/g [265]. The co-existence of other metal ions may affect the adsorption of HAP for metal ions. In the presence of Al(III), Cd(II), Cu(II), Fe(II), Ni(II), and

Zn(II) ions, the Pb(II) immobilization was inhibited by co-existing ions, and the removal efficiency of Pb(II) is in the range of 37–100% for different co-existence ions, with the effect order: Al(III) > Cu(II) > Fe(II) > C d(II) > Zn(II) > Ni(II) and Cu(II) > Fe(II) > Cd(II) > Zn(II) > Al(III) > Ni(I I) at high and low initial Pb(II) concentration, respectively [266].

The adsorption properties of HAP for different matters can be improved by surface organo-modification, inorganic modification, or forming composite with other components. The chitosan (CS) with abundant resource, better biocompatibility, and enough active sites (-NH_2 and OH) was regarded as the promising candidate to prepare a porous CS/HAP membrane with a sponge-like structure, a three-dimensional interpenetrated morphology, and a mean pore size <10 μm [267]. The composite has excellent dye adsorption capacity higher than commercial activate carbon about four times, and 98% of removal ratio was achieved within 15 min. The HAP modified by the Co(II) and ferrocyanide (HAFC) showed excellent removal behavior for strontium and cesium ions from solution [268] due to the ion-exchange mechanism. The Si-substituted carbonate HAP prepared through the hybrid of silicate and carbonate with HAP originating from the egg-shell via sonochemistry co-precipitation showed the maximal Cu(II) adsorption capacity of 246.80 mg/g at pH 5.7 and 90 min under a temperature of 313 K [95]. As for the composite of HAP with other components, Khanday et al. [269,270] synthesized mesoporous zeolite-HAP-activated palm ash (*Z*-HAP-AA) composite using oil palm ash and electric arc furnace steel slag as starting material via a hydrothermal process. The Ca/P ratio and SiO_2/Al_2O_3 ratio in the resultant HAP and zeolite-X product are 1.667 and 3, respectively. The optimal composite Z-HAP-AA-1:3 was regarded as a suitable adsorbent to adsorb tetracycline with the maximum monolayer adsorption capacity of 244.63 mg/g. In addition to introducing the component with adsorption activity, the loading of magnetic materials on HAP make it easy to be separated and recycled from the solution after adsorption. The magnetic HAP-immobilized oxidized multi-walled carbon nanotubes were regarded as a potential adsorbent for removal of Pb(II) and methylene blue (MB) with the maximum adsorption capacity of 698.4 mg/g for Pb(II) and 328.4 mg/g for MB, respectively [271].

In addition to the adsorption of HAP for usual pollutants, HAP was also used for adsorption of some nutrient substances [272]. It has been confirmed that HAP can be used for the adsorption of bovine serum albumin (BSA) with the maximum protein adsorption amount of (1.54 mg m^{-2}); the affinity constant (678.8 L g^{-1}) increased with the decline of pH, implying that electrostatic and hydration effects were significant for adsorption of BSA on HAP [273].

In the separation field, HAP was well used for purification of water. HAP was incorporated into cellulose acetate to form a nanocomposite membrane. The HAP nanoparticles were present on the surface of

the membrane. The existence of HAP was found to affect the hydrodynamic property of the composite membrane, resulting in a more stable hydrodynamic process, and the flow variation in time was much lower compared to the membrane of cellulose acetate [274].

10.3.7 Sensors

Sensors, common devices, play an irreplaceable role in human producing and living. There are many kinds of sensors, such as biosensors toward drugs and alcohol [275–278], smart sensors used to fire alarms [279] as well as electrochemical detectors and gas-sensors applied to the detection of organic or inorganic contaminates [280–283]. However, the traditional sensors usually have inferior sensitivity, mechanical strength, and thermal stability, leading to a short service life. So, development of new sensors has aroused considerable attention. Wang et al. [284] synthesized a novel H_2O_2 biosensor through the electron transfer of incorporated horseradish peroxidase (HRP) onto silica-HAP hybrid film-modified glassy carbon electrode (GCE). The as-prepared biosensor showed a well electrocatalytic response toward the reduction of H_2O_2 without the assistance of an electron mediator, which also exhibited the better reproducibility and strong sensitivity toward H_2O_2 with the detection limit of 0.35 μM. The Michaelis-Menten constant (k_m^{app}) of the sensor was 21.8 μM, suggesting a high enzymatic activity for H_2O_2. The CO_2 gas-sensor was developed based on the electrical conductivity changes originating from porous HAP ceramics, which had fundamental sensor properties [285]. The quartz crystal microbalance with dissipation (QCM-D) sensor from the ultra-thin layer of nanosize HAP was prepared, which showed high stability and sensitivity for detection of protein adsorption [286]. The potentiometric sensor was developed from HAP for the detection of phosphate [287], and the electrode showed a high linear response range from 5.0×10^{-5} to 5.0×10^{-2} mol/L, with a slope of 33 mV decade^{-1} and a detection limit of 2.5×10^{-5} mol/L. In order to achieve the analysis of l-tyrosine, Kanchana et al. developed a new biosensor based on Fe-doped HAP (Fe-HA) nanocrystal and tyrosinase via a facile microwave irradiation technique. The obtained biosensor Fe-HA/tyrosinase showed a linear response to l-tyrosine toward a wide concentration range of 1.0×10^{-7} to 1.0×10^{-5} M with a detection limit of 245 nM at pH 7.0. Moreover, the sensor also exhibited an admired selectivity, well reproducibility, and stability as well as anti-interference for the determination of l-tyrosine [288].

It is significant for the environmental and transport agency to invent an effective detection device over the family of alcohol. Anjum et al. developed a graphite-doped calcium HAP (GHAP) nano ceramic composite by liquid phase reinforce technique, and different composite of graphite were doped in HAP to prepare the sensor used to the

detection of alcohol (i.e., methanol, ethanol, and propanol) at a lower concentration (100 ppm). Compared with HAP and graphite-doped HAP materials, the dopant significantly improved the detection of volatile pollutant (VOCs), with six fold higher sensitivity toward alcoholic vapors for GHAP than the HAP [289]. As for the detection of heavy metal ions, the electrochemical sensor based on an indium tin oxide (ITO) glass electrode modified with HAP (HAP) film was prepared by an electrodeposited technique, which was used to simultaneously detect the Pb^{2+}, Cu^{2+}, and Hg^{2+} by using the differential pulse voltammetry (DPV) method. The limits of detection (S/N = 3) were 1×10^{-12}, 1×10^{-12}, 8×10^{-8} M for Pd^{2+}, Cu^{2+}, and Hg^{2+}, respectively [290].

10.3.8 Fire Resistance

Over the past years, fire-resistant materials have gotten an enormous development in view of the extensive demands in various fields, such as papermaking [291], furniture/wood [292], battery [293], and military projects. HAP, as an available fire-resistant material, has exhibited good application prospects due to its advantages, including easily obtained, porosity, high-mechanical property, and good thermal stability. Various flexible fire-resistant HAP-ordered architectures were constructed by using the self-assembled highly ordered ultra-long HAP nanowires, which can be applied in high-strength and highly flexible nanorope, highly flexible textile, and 3-D printed pattern [294]. The ultra-long HAP nanowires can be generated from nanoscale to microscale then to macroscale, and the structure of HAP was controllable. The incorporation of HAP nanomaterials may not only improve the flexibility and mechanical strength of cellulose fibers, but the thermal stability also may resist temperatures as high as 700°C, which enable the materials to be used as fire-resistant porous separators to guarantee the safety of batteries [293]. The HAP can be introduced into cellulose paper to improve its flame-resistant ability, liquid repellency to various commercial drinks, and self-cleaning properties [295]. The addition of HAP leads to an obvious increase of strength, flexibility and fire-resistant capability of paper, and the experimental results revealed the tensile strength of the HAP-containing inorganic paper reached to ≈15 MPa [296]. The fire-resistance property and mechanical properties of polyester resin materials [297] and PVA-HAP aerogel [298] were enhanced after incorporating HAP, and the HAP is superior to the conventional antimony trioxide filler or those reported by state-of-the-art foams, respectively.

10.3.9 Coating

The well-known method that has been used to coat HAP on the surface of implanting materials (metallic) is sputter coating, which

includes dip coating, pulsed-laser deposition, hot pressing and hot isostatic pressing, thermal spraying, electrostatic spraying, electrophoretic deposition, solution gel, pulse laser deposition, and an electrostatic layer-by-layer sputtering method [299,300]. Daugaard et al. [301] evaluated the mechanical fixation and tissue response to implants coated with the well-documented plasma-sprayed HAP coating, and two new alternative thinner HAP coatings: one is electrochemical-assisted deposited HAP and biomimetic coating combining cold electrochemical-assisted deposition of HAP. The results showed that HAP coatings, deposited either by a plasma-spray technique or electrochemically, increases the mechanical fixation and bone ongrowth. Compared to the required sophisticated vacuum systems and apparatus of most methods excluding plasma-spray deposition, sol-gel dip along with coating and electrochemical deposition are widely applied to metal implants. Both of the processes are similar and have been classified to be relatively low-cost and easier methods compared to others [302]. Wang et al. [303] deposited FHAP and HAP coatings on Ti substrates by an electrochemical-deposition technique. All the coatings were phase-pure, homogenous, and had a thickness of 5 μm after heat treatment. The surface morphologies of the coatings are represented in Fig. 10.7. The neat HAP coating consisted of thin

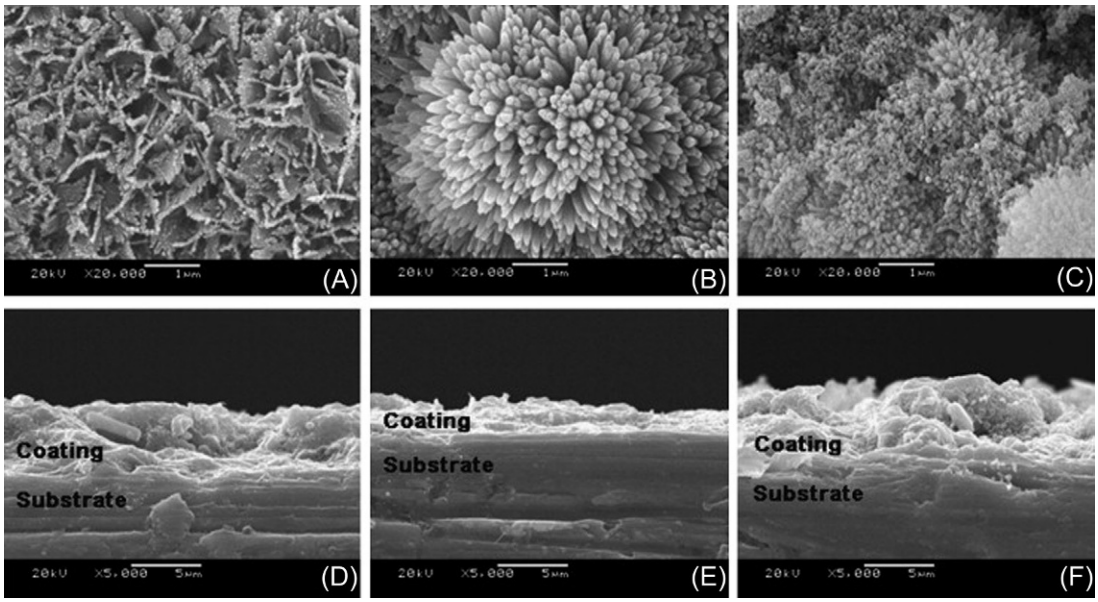

Fig. 10.7 SEM micrographs of apatite coatings after vacuum calcination. Surface morphologies: (A) HAP, (B) FHAP0.004 and (C) FHAP0.012; cross-sectional morphologies: (D) HAP, (E) FHAP0.004 and (F) FHAP0.012. Pictures of all FHAP coatings are representatively shown by those of FHAP0.004 and FHAP0.012 specimens. Reproduced with permission from J. Wang, Y. Chao, Q. Wan, Z. Zhu, H. Yu, Fluoridated hydroxyapatite coatings on titanium obtained by electrochemical deposition, Acta Biomater. 5 (5) (2009) 1798–1807.

flakes, which developed perpendicularly to the substrate (Fig. 10.7A). Adjacent curled flakes fused together on one joint to construct the microporous structure with pore diameter of about 1 μm. FHAP coatings appeared sharply different in that they were much denser and smoother than HAP coatings.

Two different coatings were built using both spin and dip processes. The TiO_2/HAP bilayer formed by deposition of outer HAP layer and inner TiO_2 layer, revealed unsatisfactory structural features, including bonding failure and surface delamination along with a high-surface roughness, leading to lack of stem cell adhesion. In contrast, the TiO_2/HAP composite exhibited better structure features and biocompatible properties. Moreover, the TiO_2/HAP composite improved the corrosion resistance of the 316 L SS implant and showed mechanical properties close to that of hard tissue once incubated in physiological conditions for 7 days, highlighting its potential application in hard-tissue replacement [304]. Rigo et al. [305] obtained a silicon nitride with bioactive surface characteristic, using the biomimetic method with a sodium silicate solution as nucleant agent. Silicon nitride has good mechanical strength, but it has limited biomedical applications due to its inertness. The obtained results showed that the biomimetic method promoted the deposition of a dense layer of HAP on silicon nitride surfaces. However, the strength of HAP coatings to withstand physiological loads without fragmentation and the issues related to third-body wear by HAP particles restrict its applicability [306].

10.3.10 Nanopaper

Conventional paper made from plant cellulose fibers is easily destroyed by liquid or fire. Moreover, the production of paper leads to severe environmental problems. In view of the flammability and toxicity of organics, Chen et al. constructed the inorganic fire-resistant paper originating from biocompatible ultra-long HAP nanowires with the surface modification of sodium oleate. The as-prepared paper possesses the free-standing, highly flexible, superhydrophobic, and good fire-resistant properties and laminar structure. It was worth noting that the laminar structure can enormously enhance the resistance of paper from mechanical destruction. Such nanopapers show interesting mechanical properties, optical transparency, and a smooth surface [307] together with the possibility of combining with another kind of nanoparticle [308,309] as well as the incorporation of different functional groups on their surface [310,311]. Paper-like materials made from pure inorganic components have rarely been reported [312]. In general, materials for producing paper should be white in color, nontoxic, highly flexible, and easy to make into thin membranes; however, few inorganic materials can meet these requirements. Lu et al. [313]

reported a new method to fabricate highly flexible and nonflammable inorganic HAP paper by using ultra-long HAP nanowires with high-aspect ratios. The HAP nanopaper is highly flexible and nonflammable, and it can be bent and rolled without visible damage, which enables it to be used as printing or writing paper with excellent nonflammability and high thermal stability. It also has properties for permanent and safe storage of information, such as for archives and important documents. In addition, HAP paper has a good performance as an adsorbent for organic pollutants. Fig. 10.8A shows a square of HAP nanopaper with a length of 108 mm. The HAP nanopaper has high flexibility, which means it can be laid flat (Fig. 10.8B), bent (Fig. 10.8C), or rolled (Fig. 10.8D) without visible damage.

A new kind of ultra-long HAP nanowire (HAPNW)-based paper was prepared, benefiting from the luminescence ability of doped lanthanide ions and the high flexibility of nanopapers. The nanopaper exhibits unique luminescence properties, tunable emission color, writability, and good processability [291]. In addition, the ultra-long HAP nanowires-based nanopaper can be used as a supporter of nano silver and ciprofloxacin to form new kinds of high-performance antibacterial material [314]. In a word, the HAP-based nanopaper exhibits high flexibility, mesoporous pores, high drug-loading capacity, sustained and pH-responsive release properties, good antibacterial activity, and good biocompatibility, which greatly extended the application fields of HAP.

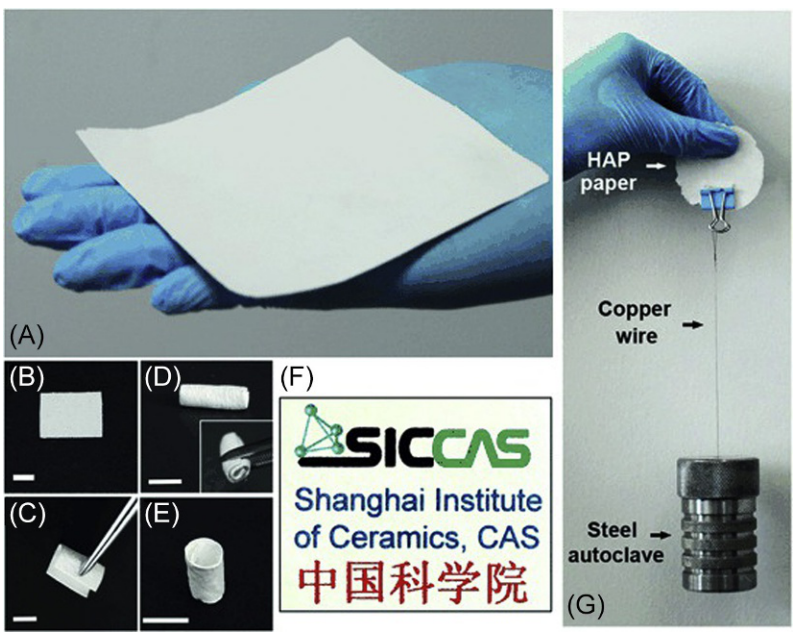

Fig. 10.8 Photographs of the as-prepared highly flexible and nonflammable inorganic HAP paper. (A) A sheet of HAP paper with a length of 108 mm. (B–E) The HAP paper shows a great flexibility; scale bars in (B–D) are 5 mm. (E) A hollow cylindrical HAP scaffold obtained by heating rolled HAP paper at 1000 °C for 4 h; scale bar is 20 mm. (F) English words and Chinese characters with different colors have been printed on the HAP paper by using a commercial ink-jet printer. (G) A piece of HAP paper (diameter ~5 cm, thickness ≈ 0.3 mm) made from ultra-long HAP nanowires and Na_2SiO_3 as an inorganic binder to enhance its strength; this HAP paper is able to withstand the weight of a steel autoclave (~450 g) without breaking. Reproduced with permission from B. Lu, Y. Zhu, F. Chen, Highly flexible and nonflammable inorganic hydroxyapatite paper, Chem. Eur. J. 20 (5) (2014) 1242–1246.

10.4 Conclusion and Perspectives

HAP is a well-known nanomaterial with unique crystal and chemical structure, simple and controllable synthesis method, diverse shapes, excellent osteoinductive ability, biocompatibility, and biological activity as well as non-toxic, non-immunogenic, and degradable advantages, so it plays an irreplaceable role in functional materials, especially biomedical and tissue engineering materials. In addition, HAP has certain surface activity, good adsorption and ion exchange properties, and can be modified easily by a variety of methods such as doping, loading, and surface-grafting reaction, which enable it to be widely used in many fields of adsorption, catalysis, and others. With the rapid development of nanoscience and nanotechnology, great efforts have been gradually made to synthesize new types of HAP with special morphologies in order to enrich the families of HAP-based functional materials and expand the application fields of HAP. More synthesis routes should be developed to synthesize HAP nanomaterials on a large scale to meet the requirement of the practical applications.

Although various forms of HAP have been synthesized, such as nanoparticles, nanorods, nanotubes, nanowires, hollow microspheres, hollow capsules, nanosheets, core-shell structures, and assembly structures, the mineralization process and formation mechanism should be studied further. In addition, the study on the HAP-derived materials should be intensified. The replacement of Ca by other metal ions can produce new materials with tunable properties, but the related research is still limited, and the controllable regulation of HAP structure has not been achieved. In other words, the chemical process of simulating the mineralization of natural HAP with multi-ordered structures remains a significant challenge. HAP is a multifunctional composite material that satisfies a variety of complex application scenarios. For example, the application of HAP to biomimetic regenerated bone materials, maintaining excellent osteogenic activity, preventing bacterial infection during application, and maintaining the mechanical properties of the material itself are all issues to be considered. HAP and other materials work together to take advantage of their respective advantages to solve these problems and broadening their application range is already on the agenda. This requires multidisciplinary and collaborative innovation in materials science, chemistry, physics, biology, and medicine. It can be concluded from the previous research works that HAP and clay minerals have similar performances and different advantages; there is potential to develop new functional materials with the synergistic advantages of clay minerals and HAP. This will extend the applications of clay minerals and HAP materials in advanced materials, such as biomedical materials, tissue engineering materials, and energy materials, etc.

Acknowledgments

This work was supported by the Youth Innovation Promotion Association CAS (2016370), the Key Research & Development Project of Gansu Provincial Sci. & Tech. Department, China (17YF1WA167), the Major Projects of the Natural Science Foundation of Gansu, China (18JR4RA001), and the Funds for Creative Research Groups of Gansu, China (17JR5RA306).

References

[1] M. Qi, K. He, Z. Huang, R. ShahbazianYassar, G. Xiao, Y. Lu, T. Shokuhfar, Hydroxyapatite fibers: a review of synthesis methods, J. Oral Maxillofac. Surg. 69 (8) (2017) 1354–1360.

[2] J.D. Pasteris, B. Wopenka, E. Valsami-Jones, Bone and tooth mineralization: why apatite? Elements 4 (2) (2008) 97–104.

[3] B. Wopenka, J.D. Pasteris, A mineralogical perspective on the apatite in bone, Mater. Sci. Eng. C 25 (2) (2005) 131–143.

[4] M.I. Kay, R.A. Young, A.S. Posner, Crystal structure of hydroxyapatite, Nature 204 (1964) 1050.

[5] V. Uskoković, D.P. Uskoković, Nanosized hydroxyapatite and other calcium phosphates: chemistry of formation and application as drug and gene delivery agents, J. Biomed. Mater. Res. B Appl. Biomater. 96 (1) (2011) 152–191.

[6] J.M. Hughes, J. Rakovan, The crystal structure of apatite, $Ca_5(PO_4)_3(F,OH,Cl)$, Rev. Mineral. Geochem. 48 (1) (2002) 1–12.

[7] A. Haider, S. Haider, S.S. Han, I.K. Kang, Recent advances in the synthesis, functionalization and biomedical applications of hydroxyapatite: a review, RSC Adv. 7 (13) (2017) 7442–7458.

[8] M. Sadat-Shojai, M.T. Khorasani, E. Dinpanah-Khoshdargi, A. Jamshidi, Synthesis methods for nanosized hydroxyapatite with diverse structures, Acta Biomater. 9 (8) (2013) 7591–7621.

[9] B.N. Bhattacharjee, V.K. Mishra, S.B. Rai, O. Parkash, D. Kumar, Study of morphological behavior of hydroxyapatite, EDTA hydroxyapatite and metal doped EDTA hydroxyapatite synthesized by chemical co-precipitation method via hydrothermal route, Key Eng. Mater. 720 (2017) 210–214.

[10] H. Liu, T. Chin, L. Lai, S. Chiu, K. Chung, C. Chang, M. Lui, Hydroxyapatite synthesized by a simplified hydrothermal method, Ceram. Int. 23 (1) (1997) 19–25.

[11] C. Silva, M. Graça, M. Valente, A. Sombra, Crystallite size study of nanocrystalline hydroxyapatite and ceramic system with titanium oxide obtained by dry ball milling, J. Mater. Sci. 42 (11) (2007) 3851–3855.

[12] A. Fahami, R. Ebrahimi-Kahrizsangi, B. Nasiri-Tabrizi, Mechanochemical synthesis of hydroxyapatite/titanium nanocomposite, Solid State Sci. 13 (1) (2011) 135–141.

[13] C. Mochales, R.M. Wilson, S.E. Dowker, M.P. Ginebra, Dry mechanosynthesis of nanocrystalline calcium deficient hydroxyapatite: structural characterisation, J. Alloys Compd. 509 (27) (2011) 7389–7394.

[14] B. Nasiri-Tabrizi, P. Honarmandi, R. Ebrahimi-Kahrizsangi, P. Honarmandi, Synthesis of nanosize single-crystal hydroxyapatite via mechanochemical method, Mater. Lett. 63 (5) (2009) 543–546.

[15] M. Fathi, E.M. Zahrani, Mechanochemical synthesis of fluoridated hydroxyapatite nanopowder, Int. J. Mod. Phys. B 22 (18-19) (2008) 3099–3106.

[16] H. El Briak-BenAbdeslam, M. Ginebra, M. Vert, P. Boudeville, Wet or dry mechanochemical synthesis of calcium phosphates? Influence of the water content on DCPD–CaO reaction kinetics, Acta Biomater. 4 (2) (2008) 378–386.

[17] M. Fathi, E.M. Zahrani, Mechanical alloying synthesis and bioactivity evaluation of nanocrystalline fluoridated hydroxyapatite, J. Cryst. Growth 311 (5) (2009) 1392–1403.
[18] B. Yeong, X. Junmin, J. Wang, Mechanochemical synthesis of hydroxyapatite from calcium oxide and brushite, J. Am. Ceram. Soc. 84 (2) (2001) 465–467.
[19] P. Honarmandi, P. Honarmandi, A. Shokuhfar, B. Nasiri-Tabrizi, R. Ebrahimi-Kahrizsangi, Milling media effects on synthesis, morphology and structural characteristics of single crystal hydroxyapatite nanoparticles, Adv. Appl. Ceram. 109 (2) (2010) 117–122.
[20] M. Vallet-Regi, J.M. González-Calbet, Calcium phosphates as substitution of bone tissues, Prog. Solid State Chem. 32 (1-2) (2004) 1–31.
[21] D.W. Kim, I.S. Cho, J.Y. Kim, H.L. Jang, G.S. Han, H.E. Ryu, H. Shin, H.S. Jung, H. Kim, K.S. Hong, Simple large-scale synthesis of hydroxyapatite nanoparticles: in situ observation of crystallization process, Langmuir 26 (1) (2009) 384–388.
[22] S. Koutsopoulos, K. Barlos, D. Gatos, E. Dalas, The effect of various Prothymosin α fragments on the crystal growth of hydroxyapatite in aqueous solution, J. Cryst. Growth 267 (1-2) (2004) 306–311.
[23] Y. Zhang, L. Zhou, D. Li, N. Xue, X. Xu, J. Li, Oriented nano-structured hydroxyapatite from the template, Chem. Phys. Lett. 376 (3-4) (2003) 493–497.
[24] H. Zhang, Y. Yan, Y. Wang, S. Li, Morphology and formation mechanism of hydroxyapatite whiskers from moderately acid solution, Mater. Res. 6 (1) (2003) 111–115.
[25] T. Ikoma, A. Yamazaki, S. Nakamura, M. Akao, Preparation and structure refinement of monoclinic hydroxyapatite, J. Solid State Chem. 144 (2) (1999) 272–276.
[26] S. Catros, F. Guillemot, E. Lebraud, C. Chanseau, S. Perez, R. Bareille, J. Amédée, J.C. Fricain, Physico-chemical and biological properties of a nano-hydroxyapatite powder synthesized at room temperature, IRBM 31 (4) (2010) 226–233.
[27] Y. Zhang, J. Lu, A mild and efficient biomimetic synthesis of rodlike hydroxyapatite particles with a high aspect ratio using polyvinylpyrrolidone as capping agent, Cryst. Growth Des. 8 (7) (2008) 2101–2107.
[28] S. Swain, D. Sarkar, A comparative study: hydroxyapatite spherical nanopowders and elongated nanorods, Ceram. Int. 37 (7) (2011) 2927–2930.
[29] A. Afshar, M. Ghorbani, N. Ehsani, M. Saeri, C. Sorrell, Some important factors in the wet precipitation process of hydroxyapatite, Mater. Des. 24 (3) (2003) 197–202.
[30] L. Kong, J. Ma, F. Boey, Nanosized hydroxyapatite powders derived from coprecipitation process, J. Mater. Sci. 37 (6) (2002) 1131–1134.
[31] M. Sadat-Shojai, M.T. Khorasani, A. Jamshidi, S. Irani, Nano-hydroxyapatite reinforced polyhydroxybutyrate composites: a comprehensive study on the structural and in vitro biological properties, Mater. Sci. Eng. C 33 (5) (2013) 2776–2787.
[32] D.W. Kim, I.S. Cho, J.Y. Kim, H.L. Jang, G.S. Han, H.S. Ryu, H. Shin, H.S. Jung, H. Kim, K.S. Hong, Simple large-scale synthesis of hydroxyapatite nanoparticles: in situ observation of crystallization process, Langmuir 26 (1) (2009) 384–388.
[33] A.S. Fomin, S.M. Barinov, V.M. Ievlev, V.V. Smirnov, B.P. Mikhailov, S.V. Kutsev, E.K. Belonogov, N.A. Drozdova, Nanocrystalline hydroxyapatite ceramics, Inorg. Mater. 45 (10) (2009) 1193–1196.
[34] I.R. Gibson, W. Bonfield, Novel synthesis and characterization of an AB-type carbonate-substituted hydroxyapatite, J Biomed Mater Res B Appl Biomater 59 (4) (2002) 697–708.
[35] C. Verwilghen, M. Chkir, S. Rio, A. Nzihou, P. Sharrock, G. Depelsenaire, Convenient conversion of calcium carbonate to hydroxyapatite at ambient pressure, Mater. Sci. Eng. C 29 (3) (2009) 771–773.

[36] P.N. Kumta, C. Sfeir, D.H. Lee, D. Olton, D. Choi, Nanostructured calcium phosphates for biomedical applications: novel synthesis and characterization, Acta Biomater. 1 (1) (2005) 65–83.
[37] S. Koutsopoulos, Synthesis and characterization of hydroxyapatite crystals: a review study on the analytical methods, J. Biomed. Mater. Res. A 62 (4) (2010) 600–612.
[38] H.G. Zhang, Q. Zhu, Surfactant-assisted preparation of fluoride-substituted hydroxyapatite nanorods, Mater. Lett. 59 (24-25) (2005) 3054–3058.
[39] I. Gibson, S. Best, W. Bonfield, Chemical characterization of silicon-substituted hydroxyapatite, J. Biomed. Mater. Res. 44 (4) (1999) 422–428.
[40] A.C. Tas, Synthesis of biomimetic Ca-hydroxyapatite powders at 37°C in synthetic body fluids, Biomaterials 21 (14) (2000) 1429–1438.
[41] G. Zhang, J. Chen, S. Yang, Q. Yu, Z. Wang, Q. Zhang, Preparation of amino-acid-regulated hydroxyapatite particles by hydrothermal method, Mater. Lett. 65 (3) (2011) 572–574.
[42] B. Jokić, M. Mitrić, V. Radmilović, S. Drmanić, R. Petrović, D. Janaćković, Synthesis and characterization of monetite and hydroxyapatite whiskers obtained by a hydrothermal method, Ceram. Int. 37 (1) (2011) 167–173.
[43] H. Cao, Z. Lu, Z. He, W. Zhao, Hydroxyapatite nanocrystals for biomedical applications, J. Phys. Chem. C 114 (43) (2010) 18352–18357.
[44] J. Cihlar, K. Castkova, Direct synthesis of nanocrystalline hydroxyapatite by hydrothermal hydrolysis of alkylphosphates, Monatsh. Chem. 133 (6) (2002) 761–771.
[45] H. Zhang, B.W. Darvell, Synthesis and characterization of hydroxyapatite whiskers by hydrothermal homogeneous precipitation using acetamide, Acta Biomater. 6 (8) (2010) 3216–3222.
[46] H. Zhang, M. Zhang, Characterization and thermal behavior of calcium deficient hydroxyapatite whiskers with various Ca/P ratios, Mater. Chem. Phys. 126 (3) (2011) 642–648.
[47] X. Guo, P. Xiao, J. Liu, Z. Shen, Fabrication of nanostructured hydroxyapatite via hydrothermal synthesis and spark plasma sintering, J. Am. Ceram. Soc. 88 (4) (2005) 1026–1029.
[48] I.S. Neira, F. Guitián, T. Taniguchi, T. Watanabe, M. Yoshimura, Hydrothermal synthesis of hydroxyapatite whiskers with sharp faceted hexagonal morphology, J. Mater. Sci. 43 (7) (2008) 2171–2178.
[49] M. Sadat-Shojai, M. Atai, A. Nodehi, Design of experiments (DOE) for the optimization of hydrothermal synthesis of hydroxyapatite nanoparticles, J. Braz. Chem. Soc. 22 (3) (2011) 571–582.
[50] J. Di Chen, Y. Wang, K. Wei, S. Zhang, X. Shi, Self-organization of hydroxyapatite nanorods through oriented attachment, Biomaterials 28 (14) (2007) 2275–2280.
[51] H.S. Liu, T.S. Chin, L.S. Lai, Hydroxyapatite synthesized by a simplified hydrothermal method, Ceram. Int. 23 (1) (1997) 19–25.
[52] B. Li, X. Chen, B. Guo, X. Wang, H. Fan, X. Zhang, Fabrication and cellular biocompatibility of porous carbonated biphasic calcium phosphate ceramics with a nanostructure, Acta Biomater. 5 (1) (2009) 134–143.
[53] S.K. Padmanabhan, A. Balakrishnan, M.C. Chu, J.L. Yong, T.N. Kim, S.J. Cho, Sol-gel synthesis and characterization of hydroxyapatite nanorods, Particuology 7 (6) (2009) 466–470.
[54] K.P. Sanosh, M.C. Chu, A. Balakrishnan, Y.J. Lee, T.N. Kim, S.J. Cho, Synthesis of nano hydroxyapatite powder that simulate teeth particle morphology and composition, Curr. Appl. Phys. 9 (6) (2009) 1459–1462.
[55] S.R. Ramanan, R. Venkatesh, A study of hydroxyapatite fibers prepared via sol–gel route, Mater. Lett. 58 (26) (2004) 3320–3323.

[56] T. Anee, M. Ashok, M. Palanichamy, S.N. Kalkura, A novel technique to synthesize hydroxyapatite at low temperature, Mater. Chem. Phys. 80 (3) (2003) 725–730.
[57] A.R. Kumar, S. Kalainathan, Sol–gel synthesis of nanostructured hydroxyapatite powder in presence of polyethylene glycol, Phys. B Condens. Matter 405 (13) (2010) 2799–2802.
[58] K.P. Sanosh, M.C. Chu, A. Balakrishnan, T.N. Kim, S.J. Cho, Preparation and characterization of nano-hydroxyapatite powder using sol-gel technique, Bull. Mater. Sci. 32 (5) (2009) 465–470.
[59] A. Bigi, E. Boanini, K. Rubini, Hydroxyapatite gels and nanocrystals prepared through a sol–gel process, J. Solid State Chem. 177 (9) (2004) 3092–3098.
[60] T.A. Kuriakose, S.N. Kalkura, M. Palanichamy, D. Arivuoli, K. Dierks, G. Bocelli, C. Betzel, Synthesis of stoichiometric nano crystalline hydroxyapatite by ethanol-based sol–gel technique at low temperature, J. Cryst. Growth 263 (1-4) (2004) 517–523.
[61] M.H. Fathi, A. Hanifi, V. Mortazavi, Preparation and bioactivity evaluation of bone-like hydroxyapatite nanopowder, J. Mater. Process. Technol. 202 (1-3) (2008) 536–542.
[62] H. Eshtiagh-Hosseini, M.R. Housaindokht, M. Chahkandi, Effects of parameters of sol–gel process on the phase evolution of sol–gel-derived hydroxyapatite, Mater. Chem. Phys. 106 (2-3) (2007) 310–316.
[63] M.F. Hsieh, L.H. Perng, T.S. Chin, H.G. Perng, Phase purity of sol–gel-derived hydroxyapatite ceramic, Biomaterials 22 (19) (2001) 2601–2607.
[64] A. Jillavenkatesa, D. Hoelzer, R. Condrate, An electron microscopy study of the formation of hydroxyapatite through sol-gel processing, J. Mater. Sci. 34 (19) (1999) 4821–4830.
[65] J. Chen, Y. Wang, X. Chen, L. Ren, C. Lai, W. He, Q. Zhang, A simple sol-gel technique for synthesis of nanostructured hydroxyapatite, tricalcium phosphate and biphasic powders, Mater. Lett. 65 (12) (2011) 1923–1926.
[66] N. Montazeri, R. Jahandideh, E. Biazar, Synthesis of fluorapatite–hydroxyapatite nanoparticles and toxicity investigations, Int. J. Nanomedicine 6 (2011) 197.
[67] C. Guzman Vazquez, C. Pina Barba, N. Munguia, Stoichiometric hydroxyapatite obtained by precipitation and sol gel processes, Rev. Mex. Fis. 51 (3) (2005) 284–293.
[68] S. Bose, S.K. Saha, Synthesis of hydroxyapatite nanopowders via sucrose-templated sol-gel method, J. Am. Ceram. Soc. 86 (6) (2003) 1055–1057.
[69] A. Ioiţescu, G. Vlase, T. Vlase, G. Ilia, N. Doca, Synthesis and characterization of hydroxyapatite obtained from different organic precursors by sol–gel method, J. Therm. Anal. Calorim. 96 (3) (2009) 937–942.
[70] D.M. Liu, T. Troczynski, W.J. Tseng, Water-based sol–gel synthesis of hydroxyapatite: process development, Biomaterials 22 (13) (2001) 1721–1730.
[71] M. Murray, J. Wang, C. Ponton, P. Marquis, An improvement in processing of hydroxyapatite ceramics, J. Mater. Sci. 30 (12) (1995) 3061–3074.
[72] W. Zhou, M. Wang, W. Cheung, B. Guo, D. Jia, Synthesis of carbonated hydroxyapatite nanospheres through nanoemulsion, J. Mater. Sci. Mater. Med. 19 (1) (2008) 103–110.
[73] T. Pradeesh, M. Sunny, H. Varma, P. Ramesh, Preparation of microstructured hydroxyapatite microspheres using oil in water emulsions, Bull. Mater. Sci. 28 (5) (2005) 383–390.
[74] K. Wei, Y. Wang, C. Lai, C. Ning, D. Wu, G. Wu, N. Zhao, X. Chen, J. Ye, Synthesis and characterization of hydroxyapatite nanobelts and nanoparticles, Mater. Lett. 59 (2-3) (2005) 220–225.
[75] G. Lim, J. Wang, S. Ng, L. Gan, Formation of nanocrystalline hydroxyapatite in nonionic surfactant emulsions, Langmuir 15 (22) (1999) 7472–7477.

[76] S.K. Saha, A. Banerjee, S. Banerjee, S. Bose, Synthesis of nanocrystalline hydroxyapatite using surfactant template systems: role of templates in controlling morphology, Mater. Sci. Eng. C 29 (7) (2009) 2294–2301.
[77] H. Li, M. Zhu, L. Li, C. Zhou, Processing of nanocrystalline hydroxyapatite particles via reverse microemulsions, J. Mater. Sci. 43 (1) (2008) 384–389.
[78] J. Kamieniak, A.M. Doyle, P.J. Kelly, C.E. Banks, Novel synthesis of mesoporous hydroxyapatite using carbon nanorods as a hard-template, Ceram. Int. 43 (7) (2017) 5412–5416.
[79] H.R. Ramay, M. Zhang, Preparation of porous hydroxyapatite scaffolds by combination of the gel-casting and polymer sponge methods, Biomaterials 24 (19) (2003) 3293–3302.
[80] J. Wang, L.L. Shaw, Synthesis of high purity hydroxyapatite nanopowder via sol–gel combustion process, J. Mater. Sci. Mater. Med. 20 (6) (2009) 1223–1227.
[81] Y. Yuan, C. Liu, Y. Zhang, X. Shan, Sol–gel auto-combustion synthesis of hydroxyapatite nanotubes array in porous alumina template, Mater. Chem. Phys. 112 (1) (2008) 275–280.
[82] C.W. Chen, R.E. Riman, K.S. TenHuisen, K. Brown, Mechanochemical–hydrothermal synthesis of hydroxyapatite from nonionic surfactant emulsion precursors, J. Cryst. Growth 270 (3-4) (2004) 615–623.
[83] E. Abdel-Aal, A. El-Midany, H. El-Shall, Mechanochemical–hydrothermal preparation of nano-crystallite hydroxyapatite using statistical design, Mater. Chem. Phys. 112 (1) (2008) 202–207.
[84] T. Tian, D. Jiang, J. Zhang, Q. Lin, Synthesis of Si-substituted hydroxyapatite by a wet mechanochemical method, Mater. Sci. Eng. C 28 (1) (2008) 57–63.
[85] N.Y. Mostafa, Characterization, thermal stability and sintering of hydroxyapatite powders prepared by different routes, Mater. Chem. Phys. 94 (2-3) (2005) 333–341.
[86] X. Liu, K. Lin, J. Chang, Modulation of hydroxyapatite crystals formed from α-tricalcium phosphate by surfactant-free hydrothermal exchange, CrystEngComm 13 (6) (2011) 1959–1965.
[87] S.P. Parthiban, I.Y. Kim, K. Kikuta, C. Ohtsuki, Effect of ammonium carbonate on formation of calcium-deficient hydroxyapatite through double-step hydrothermal processing, J. Mater. Sci. Mater. Med. 22 (2) (2011) 209–216.
[88] X. Zhang, K.S. Vecchio, Hydrothermal synthesis of hydroxyapatite rods, J. Cryst. Growth 308 (1) (2007) 133–140.
[89] M. Ashok, S.N. Kalkura, N.M. Sundaram, D. Arivuoli, Growth and characterization of hydroxyapatite crystals by hydrothermal method, J. Mater. Sci. Mater. Med. 18 (5) (2007) 895–898.
[90] S. Banerjee, B. Bagchi, S. Bhandary, A. Kool, N.A. Hoque, P. Biswas, K. Pal, P. Thakur, K. Das, P. Karmakar, Antimicrobial and biocompatible fluorescent hydroxyapatite-chitosan nanocomposite films for biomedical applications, Colloids Surf. B: Biointerfaces 171 (2018) 300–307.
[91] P. Shuk, W.L. Suchanek, T. Hao, E. Gulliver, R.E. Riman, M. Senna, K.S. TenHuisen, V.F. Janas, Mechanochemical-hydrothermal preparation of crystalline hydroxyapatite powders at room temperature, J. Mater. Res. 16 (5) (2001) 1231–1234.
[92] E. White, E. Shors, Biomaterial aspects of Interpore-200 porous hydroxyapatite, Dent. Clin. N. Am. 30 (1) (1986) 49–67.
[93] R.E. Holmes, R. Bucholz, V. Mooney, Porous hydroxyapatite as a bone-graft substitute in metaphyseal defects. A histometric study, J. Bone Joint Surg. Am. 68 (6) (1986) 904–911.
[94] D.M. Roy, S.K. Linnehan, Hydroxyapatite formed from coral skeletal carbonate by hydrothermal exchange, Nature 247 (5438) (1974) 220.
[95] R. Zeng, W. Tang, X. Liu, C. Ding, D. Gong, Adsorption of Zn^{2+} from aqueous solutions by si-substituted carbonated hydroxylapatite: equilibrium, kinetics, and mechanisms, Environ. Prog. Sustain. Energy 37 (6) (2018) 2073–2081.

[96] M. Roudan, S. Ramesh, Y. Wong, H. Chandran, S. Krishnasamy, W. Teng, L. Bang, Sintering behavior and characteristic of bio-based hydroxyapatite coating deposited on titanium, J. Ceram. Process. Res. 18 (9) (2017) 640–645.
[97] M. Sivakumar, T.S. Kumar, K. Shantha, K.P. Rao, Development of hydroxyapatite derived from Indian coral, Biomaterials 17 (17) (1996) 1709–1714.
[98] R. Holmes, V. Mooney, R. Bucholz, A. Tencer, A coralline hydroxyapatite bone graft substitute. preliminary report, Clin. Orthop. Relat. Res. 188 (1984) 252–262.
[99] I. Mobasherpour, M.S. Heshajin, A. Kazemzadeh, M. Zakeri, Synthesis of nanocrystalline hydroxyapatite by using precipitation method, J. Alloys Compd. 430 (1-2) (2007) 330–333.
[100] Q. Hu, B. Li, M. Wang, J. Shen, Preparation and characterization of biodegradable chitosan/hydroxyapatite nanocomposite rods via in situ hybridization: a potential material as internal fixation of bone fracture, Biomaterials 25 (5) (2004) 779–785.
[101] S. Koutsopoulos, Synthesis and characterization of hydroxyapatite crystals: a review study on the analytical methods, J. Biomed. Mater. Res. 62 (4) (2002) 600–612.
[102] A.L. Boskey, A.S. Posner, Conversion of amorphous calcium phosphate to microcrystalline hydroxyapatite. A pH-dependent, solution-mediated, solid-solid conversion, J. Phys. Chem. 77 (19) (1973) 2313–2317.
[103] G.K. Hunter, P.V. Hauschka, R.A. Poole, L.C. Rosenberg, H.A. Goldberg, Nucleation and inhibition of hydroxyapatite formation by mineralized tissue proteins, Biochem. J. 317 (1) (1996) 59–64.
[104] H. Yang, L. Hao, N. Zhao, C. Du, Y. Wang, Hierarchical porous hydroxyapatite microsphere as drug delivery carrier, CrystEngComm 15 (29) (2013) 5760–5763.
[105] T. Matsumoto, M. Okazaki, A. Nakahira, J. Sasaki, H. Egusa, T. Sohmura, Modification of apatite materials for bone tissue engineering and drug delivery carriers, Curr. Med. Chem. 14 (25) (2007) 2726–2733.
[106] Y.T. Huang, M. Imura, Y. Nemoto, C.H. Cheng, Y. Yamauchi, Block-copolymer-assisted synthesis of hydroxyapatite nanoparticles with high surface area and uniform size, Sci. Technol. Adv. Mater. 12 (4) (2011) 045005.
[107] S. Dasgupta, S.S. Banerjee, A. Bandyopadhyay, S. Bose, Zn-and Mg-doped hydroxyapatite nanoparticles for controlled release of protein, Langmuir 26 (7) (2010) 4958–4964.
[108] H. Wu, T. Wang, M.C. Bohn, F. Lin, M. Spector, Novel magnetic hydroxyapatite nanoparticles as non-viral vectors for the glial cell line-derived neurotrophic factor gene, Adv. Funct. Mater. 20 (1) (2010) 67–77.
[109] J. Kirkham, S.J. Brookes, R.C. Shore, S.R. Wood, D.A. Smith, J. Zhang, H. Chen, C. Robinson, Physico-chemical properties of crystal surfaces in matrix–mineral interactions during mammalian biomineralisation, Curr. Opin. Colloid Interface Sci. 7 (1-2) (2002) 124–132.
[110] S. Mondal, S.V. Dorozhkin, U. Pal, Recent progress on fabrication and drug delivery applications of nanostructured hydroxyapatite, Wiley Interdiscip. Rev. Nanomed. Nanobiotechnol. 10 (4) (2018) e1504.
[111] Y.H. Yang, C.H. Liu, Y.H. Liang, F.H. Lin, K.C.W. Wu, Hollow mesoporous hydroxyapatite nanoparticles (hmHANPs) with enhanced drug loading and pH-responsive release properties for intracellular drug delivery, J. Mater. Chem. B 1 (19) (2013) 2447–2450.
[112] Q. Zhao, T. Wang, J. Wang, L. Zheng, T. Jiang, G. Cheng, S. Wang, Template-directed hydrothermal synthesis of hydroxyapatite as a drug delivery system for the poorly water-soluble drug carvedilol, Appl. Surf. Sci. 257 (23) (2011) 10126–10133.
[113] P. Yang, Z. Quan, C. Li, X. Kang, H. Lian, J. Lin, Bioactive, luminescent and mesoporous europium-doped hydroxyapatite as a drug carrier, Biomaterials 29 (32) (2008) 4341–4347.

[114] J.S. Son, M. Appleford, J.L. Ong, J.C. Wenke, J.M. Kim, S.H. Choi, D.S. Oh, Porous hydroxyapatite scaffold with three-dimensional localized drug delivery system using biodegradable microspheres, J. Control. Release 153 (2) (2011) 133–140.
[115] Y. Mizushima, T. Ikoma, J. Tanaka, K. Hoshi, T. Ishihara, Y. Ogawa, A. Ueno, Injectable porous hydroxyapatite microparticles as a new carrier for protein and lipophilic drugs, J. Control. Release 110 (2) (2006) 260–265.
[116] Y. Zhang, K. Dong, F. Wang, H. Wang, J. Wang, Z. Jiang, S. Diao, Three dimensional macroporous hydroxyapatite/chitosan foam-supported polymer micelles for enhanced oral delivery of poorly soluble drugs, Colloids Surf. B: Biointerfaces 170 (2018) 497–504.
[117] Z. Song, Y. Liu, J. Shi, T. Ma, Z. Zhang, H. Ma, S. Cao, Hydroxyapatite/mesoporous silica coated gold nanorods with improved degradability as a multi-responsive drug delivery platform, Mater. Sci. Eng. C 83 (2018) 90–98.
[118] G.F. Andrade, J.A.Q.A. Faria, D.A. Gomes, A.L.B. de Barros, R.S. Fernandes, A.C.S. Coelho, J.A. Takahashi, A. da Silva Cunha, E.M.B. de Sousa, Mesoporous silica SBA-16/hydroxyapatite-based composite for ciprofloxacin delivery to bacterial bone infection, J. Sol-Gel Sci. Technol. 85 (2) (2018) 369–381.
[119] G.E. Poinern, R.K. Brundavanam, N. Mondinos, Z.T. Jiang, Synthesis and characterisation of nanohydroxyapatite using an ultrasound assisted method, Ultrason. Sonochem. 16 (4) (2009) 469–474.
[120] C. Hellmich, F.J. Ulm, Average hydroxyapatite concentration is uniform in the extracollagenous ultrastructure of mineralized tissues: evidence at the 1–10-μm scale, Biomech. Model. Mechanobiol. 2 (1) (2003) 21–36.
[121] M. Braddock, P. Houston, C. Campbell, P. Ashcroft, Born again bone: tissue engineering for bone repair, Physiology 16 (5) (2001) 208–213.
[122] V. Orlovskii, V. Komlev, S. Barinov, Hydroxyapatite and hydroxyapatite-based ceramics, Inorg. Mater. 38 (10) (2002) 973–984.
[123] M. Bohner, Calcium orthophosphates in medicine: from ceramics to calcium phosphate cements, Injury 31 (2000) D37–D47.
[124] S.V. Dorozhkin, Calcium orthophosphate-based biocomposites and hybrid biomaterials, J. Mater. Sci. 44 (9) (2009) 2343–2387.
[125] M.P. Ginebra, M. Espanol, E.B. Montufar, R.A. Perez, G. Mestres, New processing approaches in calcium phosphate cements and their applications in regenerative medicine, Acta Biomater. 6 (8) (2010) 2863–2873.
[126] A.J.W. Johnson, B.A. Herschler, A review of the mechanical behavior of CaP and CaP/polymer composites for applications in bone replacement and repair, Acta Biomater. 7 (1) (2011) 16–30.
[127] D. Wahl, J. Czernuszka, Collagen-hydroxyapatite composites for hard tissue repair, Eur. Cell. Mater. 11 (2006) 43–56.
[128] Y.G. Kim, D.S. Seo, J.K. Lee, Comparison of dissolution resistance in artificial hydroxyapatite and biologically derived hydroxyapatite ceramics, J. Phys. Chem. Solids 69 (5-6) (2008) 1556–1559.
[129] H. Zhou, J. Lee, Nanoscale hydroxyapatite particles for bone tissue engineering, Acta Biomater. 7 (7) (2011) 2769–2781.
[130] W. Zhu, X. Zhang, D. Wang, W. Lu, Y. Ou, Y. Han, K. Zhou, H. Liu, W. Fen, L. Peng, Experimental study on the conduction function of nano-hydroxyapatite artificial bone, IET Micro Nano Lett. 5 (1) (2010) 19–27.
[131] A. Boskey, Bone mineral crystal size, Osteoporos. Int. 14 (5) (2003) 16–21.
[132] T. Yuasa, Y. Miyamoto, K. Ishikawa, M. Takechi, Y. Momota, S. Tatehara, M. Nagayama, Effects of apatite cements on proliferation and differentiation of human osteoblasts in vitro, Biomaterials 25 (7-8) (2004) 1159–1166.
[133] R.A. Ayers, S.J. Simske, C.R. Nunes, L.M. Wolford, Long-term bone ingrowth and residual microhardness of porous block hydroxyapatite implants in humans, JOMS 56 (11) (1998) 1297–1301.

[134] N. Tamai, A. Myoui, T. Tomita, T. Nakase, J. Tanaka, T. Ochi, H. Yoshikawa, Novel hydroxyapatite ceramics with an interconnective porous structure exhibit superior osteoconduction in vivo, J. Biomed. Mater. Res. 59 (1) (2002) 110–117.
[135] E.S. Ahn, N.J. Gleason, A. Nakahira, J.Y. Ying, Nanostructure processing of hydroxyapatite-based bioceramics, Nano Lett. 1 (3) (2001) 149–153.
[136] X. Li, Q. Feng, X. Liu, W. Dong, F. Cui, Collagen-based implants reinforced by chitin fibres in a goat shank bone defect model, Biomaterials 27 (9) (2006) 1917–1923.
[137] D. Wang, Y. Han, W. Zhu, W. Lu, H. Liu, Y. Jiang, J. Xiong, J. Liu, W. Ouyang, W. Liu, Nano-hydroxyapatite artificial bone with different pore sizes to repair radial defect in rabbits, J. Clin. Rehabil. Tissue Eng. Res. 11 (48) (2007) 9641–9645.
[138] J. Zhang, J. Nie, Q. Zhang, Y. Li, Z. Wang, Q. Hu, Preparation and characterization of bionic bone structure chitosan/hydroxyapatite scaffold for bone tissue engineering, J. Biomater. Sci. Polym. Ed. 25 (1) (2014) 61–74.
[139] J. Venkatesan, S.K. Kim, Chitosan composites for bone tissue engineering—an overview, Mar. Drugs 8 (8) (2010) 2252–2266.
[140] Y. Zhang, J.R. Venugopal, A. El-Turki, S. Ramakrishna, B. Su, C.T. Lim, Electrospun biomimetic nanocomposite nanofibers of hydroxyapatite/chitosan for bone tissue engineering, Biomaterials 29 (32) (2008) 4314–4322.
[141] L. Jiang, Y. Li, X. Wang, L. Zhang, J. Wen, M. Gong, Preparation and properties of nano-hydroxyapatite/chitosan/carboxymethyl cellulose composite scaffold, Carbohydr. Polym. 74 (3) (2008) 680–684.
[142] H. Liu, H. Peng, Y. Wu, C. Zhang, Y. Cai, G. Xu, Q. Li, X. Chen, J. Ji, Y. Zhang, The promotion of bone regeneration by nanofibrous hydroxyapatite/chitosan scaffolds by effects on integrin-BMP/Smad signaling pathway in BMSCs, Biomaterials 34 (18) (2013) 4404–4417.
[143] S. Maji, T. Agarwal, J. Das, T.K. Maiti, Development of gelatin/carboxymethyl chitosan/nano-hydroxyapatite composite 3D macroporous scaffold for bone tissue engineering applications, Carbohydr. Polym. 189 (2018) 115–125.
[144] J. Venkatesan, R. Jayakumar, S. Anil, E.P. Chalisserry, R. Pallela, S.K. Kim, Development of alginate-chitosan-collagen based hydrogels for tissue engineering, J. Biomate Tissue Eng. 5 (6) (2015) 458–464.
[145] H. Luo, G. Zuo, G. Xiong, C. Li, C. Wu, Y. Wan, Porous nanoplate-like hydroxyapatite–sodium alginate nanocomposite scaffolds for potential bone tissue engineering, Mater. Technol. 32 (2) (2017) 78–84.
[146] P. Zhang, H. Wu, H. Wu, Z. Lù, C. Deng, Z. Hong, X. Jing, X. Chen, RGD-conjugated copolymer incorporated into composite of poly (lactide-co-glycotide) and poly (L-lactide)-grafted nanohydroxyapatite for bone tissue engineering, Biomacromolecules 12 (7) (2011) 2667–2680.
[147] Z. Dong, Y. Li, Q. Zou, Degradation and biocompatibility of porous nano-hydroxyapatite/polyurethane composite scaffold for bone tissue engineering, Appl. Surf. Sci. 255 (12) (2009) 6087–6091.
[148] Y. Pan, D. Xiong, F. Gao, Viscoelastic behavior of nano-hydroxyapatite reinforced poly (vinyl alcohol) gel biocomposites as an articular cartilage, J. Mater. Sci. Mater. Med. 19 (5) (2008) 1963–1969.
[149] H. Wang, Y. Li, Y. Zuo, J. Li, S. Ma, L. Cheng, Biocompatibility and osteogenesis of biomimetic nano-hydroxyapatite/polyamide composite scaffolds for bone tissue engineering, Biomaterials 28 (22) (2007) 3338–3348.
[150] L. Fang, Y. Leng, P. Gao, Processing of hydroxyapatite reinforced ultrahigh molecular weight polyethylene for biomedical applications, Biomaterials 26 (17) (2005) 3471–3478.
[151] S.K. Misra, S.P. Valappil, I. Roy, A.R. Boccaccini, Polyhydroxyalkanoate (PHA)/inorganic phase composites for tissue engineering applications, Biomacromolecules 7 (8) (2006) 2249–2258.

[152] M. Turkoz, A.O. Atilla, Z. Evis, Silver and fluoride doped hydroxyapatites: investigation by microstructure, mechanical and antibacterial properties, Ceram. Int. 39 (8) (2013) 8925–8931.
[153] D. Verret, Y. Ducic, L. Oxford, J. Smith, Hydroxyapatite cement in craniofacial reconstruction, Otolaryngol. Head Neck Surg. 133 (6) (2005) 897–899.
[154] D. Aronov, A. Karlov, G. Rosenman, Hydroxyapatite nanoceramics: basic physical properties and biointerface modification, J. Eur. Ceram. Soc. 27 (13-15) (2007) 4181–4186.
[155] J.R. You, J.H. Seo, Y.H. Kim, W.C. Choi, Six cases of bacterial infection in porous orbital implants, Jpn. J. Ophthalmol. 47 (5) (2003) 512–518.
[156] M. Mirzaee, M. Vaezi, Y. Palizdar, Synthesis and characterization of silver doped hydroxyapatite nanocomposite coatings and evaluation of their antibacterial and corrosion resistance properties in simulated body fluid, Mater. Sci. Eng. C 69 (2016) 675–684.
[157] D. Predoi, C.L. Popa, P. Chapon, A. Groza, S.L. Iconaru, Evaluation of the antimicrobial activity of different antibiotics enhanced with silver-doped hydroxyapatite thin films, Materials 9 (9) (2016) 778.
[158] C. Wilcock, G. Stafford, C. Miller, Y. Ryabenkova, M. Fatima, P. Gentile, G. Möbus, P. Hatton, Preparation and antibacterial properties of silver-doped nanoscale hydroxyapatite pastes for bone repair and augmentation, J. Biomed. Nanotechnol. 13 (9) (2017) 1168–1176.
[159] R. Shamsudin, M.H. Ng, A. Ahmad, M.A.M. Akbar, Z. Rashidbenam, Silver-doped pseudowollastonite synthesized from rice husk ash: antimicrobial evaluation, bioactivity and cytotoxic effects on human mesenchymal stem cells, Ceram. Int. 44 (10) (2018) 11381–11389.
[160] D. Predoi, S.L. Iconaru, M. Albu, C.C. Petre, G. Jiga, Physicochemical and antimicrobial properties of silver-doped hydroxyapatite collagen biocomposite, Polym. Eng. Sci. 57 (6) (2017) 537–545.
[161] J. Gong, L. Yang, Q. He, T. Jiao, In vitro evaluation of the biological compatibility and antibacterial activity of a bone substitute material consisting of silver-doped hydroxyapatite and Bio-Oss, J. Biomed. Mater. Res. B Appl. Biomater. 106 (1) (2018) 410–420.
[162] Y. Yang, C. Chen, J. Wang, Y. Wang, F. Lin, Flame sprayed zinc doped hydroxyapatite coating with antibacterial and biocompatible properties, Ceram. Int. 43 (2017) S829–S835.
[163] R. Sergi, D. Bellucci, R.T. Candidato Jr., L. Lusvarghi, G. Bolelli, L. Pawlowski, G. Candiani, L. Altomare, L. De Nardo, V. Cannillo, Bioactive Zn-doped hydroxyapatite coatings and their antibacterial efficacy against *Escherichia coli* and *Staphylococcus aureus*, Surf. Coat. Technol. 352 (2018) 84–91.
[164] Y. Huang, X. Zhang, H. Mao, T. Li, R. Zhao, Y. Yan, X. Pang, Osteoblastic cell responses and antibacterial efficacy of Cu/Zn co-substituted hydroxyapatite coatings on pure titanium using electrodeposition method, RSC Adv. 5 (22) (2015) 17076–17086.
[165] S. Samani, S. Hossainalipour, M. Tamizifar, H. Rezaie, In vitro antibacterial evaluation of sol-gel-derived Zn-, Ag-, and (Zn+Ag)-doped hydroxyapatite coatings against methicillin-resistant Staphylococcus aureus, J. Biomed. Mater. Res. A 101 (1) (2013) 222–230.
[166] F. Shi, Y. Liu, W. Zhi, D. Xiao, H. Li, K. Duan, S. Qu, J. Weng, The synergistic effect of micro/nano-structured and Cu^{2+}-doped hydroxyapatite particles to promote osteoblast viability and antibacterial activity, Biomed. Mater. 12 (3) (2017) 035006.
[167] B. Hidalgo-Robatto, M. López-Álvarez, A. Azevedo, J. Dorado, J. Serra, N. Azevedo, P. González, Pulsed laser deposition of copper and zinc doped hydroxyapatite coatings for biomedical applications, Surf. Coat. Technol. 333 (2018) 168–177.

[168] M. Hadidi, A. Bigham, E. Saebnoori, S. Hassanzadeh-Tabrizi, S. Rahmati, Z.M. Alizadeh, V. Nasirian, M. Rafienia, Electrophoretic-deposited hydroxyapatite-copper nanocomposite as an antibacterial coating for biomedical applications, Surf. Coat. Technol. 321 (2017) 171–179.
[169] Y. Li, J. Ho, C.P. Ooi, Antibacterial efficacy and cytotoxicity studies of copper (II) and titanium (IV) substituted hydroxyapatite nanoparticles, Mater. Sci. Eng. C 30 (8) (2010) 1137–1144.
[170] V. Stanić, S. Dimitrijević, D.G. Antonović, B.M. Jokić, S.P. Zec, S.T. Tanasković, S. Raičević, Synthesis of fluorine substituted hydroxyapatite nanopowders and application of the central composite design for determination of its antimicrobial effects, Appl. Surf. Sci. 290 (2014) 346–352.
[171] A. Alhilou, T. Do, L. Mizban, B.H. Clarkson, D.J. Wood, M.G. Katsikogianni, Physicochemical and antibacterial characterization of a novel fluorapatite coating, ACS Omega 1 (2) (2016) 264–276.
[172] P. Nasker, M. Mukherjee, S. Kant, S. Tripathy, A. Sinha, M. Das, Fluorine substituted nano hydroxyapatite: synthesis, bio-activity and antibacterial response study, Ceram. Int. 44 (17) (2018) 22008–22013.
[173] X. Ge, Y. Leng, C. Bao, S.L. Xu, R. Wang, F. Ren, Antibacterial coatings of fluoridated hydroxyapatite for percutaneous implants, J. Biomed. Mater. Res. A 95 (2) (2010) 588–599.
[174] N. Rameshbabu, T. Sampath Kumar, T. Prabhakar, V. Sastry, K. Murty, K. Prasad Rao, Antibacterial nanosized silver substituted hydroxyapatite: synthesis and characterization, J. Biomed. Mater. Res. A 80 (3) (2007) 581–591.
[175] N. Iqbal, M.R.A. Kadir, N.H.B. Mahmood, S. Iqbal, D. Almasi, F. Naghizadeh, H. Balaji, T. Kamarul, Characterization and biological evaluation of silver containing fluoroapatite nanoparticles prepared through microwave synthesis, Ceram. Int. 41 (5) (2015) 6470–6477.
[176] Y. Yan, X. Zhang, Y. Huang, Q. Ding, X. Pang, Antibacterial and bioactivity of silver substituted hydroxyapatite/TiO_2 nanotube composite coatings on titanium, Appl. Surf. Sci. 314 (2014) 348–357.
[177] W. Chen, S. Oh, A. Ong, N. Oh, Y. Liu, H. Courtney, M. Appleford, J. Ong, Antibacterial and osteogenic properties of silver-containing hydroxyapatite coatings produced using a sol gel process, J. Biomed. Mater. Res. A 82 (4) (2007) 899–906.
[178] R.P. Singh, M. Singh, G. Verma, S. Shukla, S. Singh, S. Singh, Structural analysis of silver doped hydroxyapatite nanopowders by Rietveld refinement, Trans. Indian Inst. Metals 70 (8) (2017) 1973–1980.
[179] K.S. Hwang, S. Hwangbo, J.T. Kim, Silver-doped calcium phosphate nanopowders prepared by electrostatic spraying, J. Nanopart. Res. 10 (8) (2008) 1337–1341.
[180] M. Riaz, R. Zia, A. Ijaz, T. Hussain, M. Mohsin, A. Malik, Synthesis of monophasic Ag doped hydroxyapatite and evaluation of antibacterial activity, Mater. Sci. Eng. C 90 (2018) 308–313.
[181] M. Qi, Z. Huang, A. Phakatkar, W. Yao, Y. Yuan, T. Foroozan, G. Xiao, R. Shahbazian Yassar, Y. Lu, T. Shokuhfar, Facile hydrothermal synthesis of antibacterial multi-layered hydroxyapatite nanostructures with superior flexibility, CrystEngComm 20 (9) (2018) 1304–1312.
[182] B.S. Moonga, D.W. Dempster, Zinc is a potent inhibitor of osteoclastic bone resorption in vitro, J. Bone Miner. Res. 10 (3) (1995) 453–457.
[183] E. Thian, T. Konishi, Y. Kawanobe, P. Lim, C. Choong, B. Ho, M. Aizawa, Zinc-substituted hydroxyapatite: a biomaterial with enhanced bioactivity and antibacterial properties, J. Mater. Sci. Mater. Med. 24 (2) (2013) 437–445.
[184] S.L. Iconaru, A.M. Prodan, N. Buton, D. Predoi, Structural characterization and antifungal studies of zinc-doped hydroxyapatite coatings, Molecules 22 (4) (2017) 604.
[185] R. Sergi, D. Bellucci, R.T. Candidato, L. Lusvarghi, G. Bolelli, L. Pawlowski, G. Candiani, L. Altomare, L. De Nardo, V. Cannillo, Bioactive Zn-doped

hydroxyapatite coatings and their antibacterial efficacy against *Escherichia coli* and *Staphylococcus aureus*, Surf. Coat. Technol. 352 (2018) 84–91.
[186] Q. Wang, P. Tang, X. Ge, P. Li, C. Lv, M. Wang, K. Wang, L. Fang, X. Lu, Experimental and simulation studies of strontium/zinc-codoped hydroxyapatite porous scaffolds with excellent osteoinductivity and antibacterial activity, Appl. Surf. Sci. 462 (2018) 118–126.
[187] J. Kolmas, E. Groszyk, D. Kwiatkowska-Różycka, Substituted hydroxyapatites with antibacterial properties, Biomed. Res. Int. 2014 (2014) 1–15.
[188] P. Yin, F. Feng, T. Lei, X. Zhong, X. Jian, Osteoblastic cell response on biphasic fluorhydroxyapatite/strontium-substituted hydroxyapatite coatings, J. Biomed. Mater. Res. A 102 (3) (2014) 621–627.
[189] L. Wang, M. Wang, M. Li, Z. Shen, Y. Wang, Y. Shao, Y. Zhu, Trace fluorine substituted calcium deficient hydroxyapatite with excellent osteoblastic activity and antibacterial ability, CrystEngComm 20 (38) (2018) 5744–5753.
[190] A. Belcarz, A. Zima, G. Ginalska, Biphasic mode of antibacterial action of aminoglycoside antibiotics-loaded elastic hydroxyapatite–glucan composite, Int. J. Pharm. 454 (1) (2013) 285–295.
[191] F. Chai, J.C. Hornez, N. Blanchemain, C. Neut, M. Descamps, H. Hildebrand, Antibacterial activation of hydroxyapatite (HA) with controlled porosity by different antibiotics, Biomol. Eng. 24 (5) (2007) 510–514.
[192] F. Zheng, S. Wang, S. Wen, M. Shen, M. Zhu, X. Shi, Characterization and antibacterial activity of amoxicillin-loaded electrospun nano-hydroxyapatite/poly (lactic-co-glycolic acid) composite nanofibers, Biomaterials 34 (4) (2013) 1402–1412.
[193] X. Lian, H. Liu, X. Wang, S. Xu, F. Cui, X. Bai, Antibacterial and biocompatible properties of vancomycin-loaded nano-hydroxyapatite/collagen/poly (lactic acid) bone substitute, Prog. Nat. Sci.: Mater. Int. 23 (6) (2013) 549–556.
[194] M. Taha, F. Chai, N. Blanchemain, C. Neut, M. Goube, M. Maton, B. Martel, H.F. Hildebrand, Evaluation of sorption capacity of antibiotics and antibacterial properties of a cyclodextrin-polymer functionalized hydroxyapatite-coated titanium hip prosthesis, Int. J. Pharm. 477 (1–2) (2014) 380–389.
[195] D. Li, Y. Gong, X. Chen, B. Zhang, H. Zhang, P. Jin, H. Li, Room-temperature deposition of hydroxyapatite/antibiotic composite coatings by vacuum cold spraying for antibacterial applications, Surf. Coat. Technol. 330 (2017) 87–91.
[196] R. Ramírez-Agudelo, K. Scheuermann, A. Gala-García, A.P.F. Monteiro, A.D. Pinzón-García, M.E. Cortés, R.D. Sinisterra, Hybrid nanofibers based on poly-caprolactone/gelatin/hydroxyapatite nanoparticles-loaded doxycycline: effective anti-tumoral and antibacterial activity, Mater. Sci. Eng. C Mater. Biol. Appl. 83 (2018) 25–34.
[197] B.S. Gholizadeh, F. Buazar, S.M. Hosseini, S.M. Mousavi, Enhanced antibacterial activity, mechanical and physical properties of alginate/hydroxyapatite bionanocomposite film, Int. J. Biol. Macromol. 116 (2018) 786–792.
[198] S. Sutha, K. Kavitha, G. Karunakaran, V. Rajendran, In-vitro bioactivity, biocorrosion and antibacterial activity of silicon integrated hydroxyapatite/chitosan composite coating on 316 L stainless steel implants, Mater. Sci. Eng. C Mater. Biol. Appl. 33 (7) (2013) 4046–4054.
[199] S. Saravanan, S. Nethala, S. Pattnaik, A. Tripathi, A. Moorthi, N. Selvamurugan, Preparation, characterization and antimicrobial activity of a bio-composite scaffold containing chitosan/nano-hydroxyapatite/nano-silver for bone tissue engineering, Int. J. Biol. Macromol. 49 (2) (2011) 188–193.
[200] A. Tripathi, S. Saravanan, S. Pattnaik, A. Moorthi, N.C. Partridge, N. Selvamurugan, Bio-composite scaffolds containing chitosan/nano-hydroxyapatite/nano-copper–zinc for bone tissue engineering, Int. J. Biol. Macromol. 50 (1) (2012) 294–299.
[201] Y. Yan, X. Zhang, C. Li, Y. Huang, Q. Ding, X. Pang, Preparation and characterization of chitosan-silver/hydroxyapatite composite coatings onTiO_2 nanotube for biomedical applications, Appl. Surf. Sci. 332 (2015) 62–69.

[202] S. Jegatheeswaran, M. Sundrarajan, PEGylation of novel hydroxyapatite/PEG/Ag nanocomposite particles to improve its antibacterial efficacy, Mater. Sci. Eng. C 51 (2015) 174–181.
[203] J. Shen, B. Jin, Y. Qi, Q. Jiang, X. Gao, Carboxylated chitosan/silver-hydroxyapatite hybrid microspheres with improved antibacterial activity and cytocompatibility, Mater. Sci. Eng. C 78 (2017) 589–597.
[204] N. Ohtsu, Y. Kakuchi, T. Ohtsuki, Antibacterial effect of zinc oxide/hydroxyapatite coatings prepared by chemical solution deposition, Appl. Surf. Sci. 445 (2018) 596–600.
[205] D. Sivaraj, K. Vijayalakshmi, Novel synthesis of bioactive hydroxyapatite/f-multiwalled carbon nanotube composite coating on 316L SS implant for substantial corrosion resistance and antibacterial activity, J. Alloys Compd. 777 (2018) 1340–1346.
[206] W.Z. Yu, Y. Zhang, X. Liu, Y. Xiang, Z. Li, S. Wu, Synergistic antibacterial activity of multi components in lysozyme/chitosan/silver/hydroxyapatite hybrid coating, Mater. Des. 139 (2018) 351–362.
[207] T. Shen, W. Yang, X. Shen, W. Chen, B. Tao, X. Yang, J. Yuan, P. Liu, K. Cai, Polydopamine-assisted hydroxyapatite and lactoferrin multilayer on titanium for regulating bone balance and enhancing antibacterial property, ACS Biomater Sci. Eng. 4 (9) (2018) 3211–3223.
[208] K. Priya, G. Buvaneswari, Apatite phosphates containing heterovalent cations and their application in Knoevenagel condensation, Mater. Res. Bull. 44 (6) (2009) 1209–1213.
[209] M.K. Pillai, S. Singh, S.B. Jonnalagadda, Solvent-free Knoevenagel condensation over cobalt hydroxyapatite, Synth. Commun. 40 (24) (2010) 3710–3715.
[210] A. Solhy, R. Tahir, S. Sebti, R. Skouta, M. Bousmina, M. Zahouily, M. Larzek, Efficient synthesis of chalcone derivatives catalyzed by re-usable hydroxyapatite, Appl. Catal. A Gen. 374 (1) (2010) 189–193.
[211] M. Gruselle, T. Kanger, R. Thouvenot, A. Flambard, K. Kriis, V. Mikli, R. Traksmaa, B. Maaten, K. Tõnsuaadu, Calcium hydroxyapatites as efficient catalysts for the michael C–C bond formation, ACS Catal. 1 (12) (2011) 1729–1733.
[212] V. Polshettiwar, A. Decottignies, C. Len, A. Fihri, Suzuki-Miyaura cross-coupling reactions in aqueous media: green and sustainable syntheses of biaryls, ChemSusChem 3 (5) (2010) 502–522.
[213] K. Mori, T. Hara, T. Mizugaki, K. Ebitani, K. Kaneda, Hydroxyapatite-supported palladium nanoclusters: a highly active heterogeneous catalyst for selective oxidation of alcohols by use of molecular oxygen, J. Am. Chem. Soc. 126 (34) (2004) 10657–10666.
[214] A. Hu, M. Li, C. Chang, D. Mao, Preparation and characterization of a titanium-substituted hydroxyapatite photocatalyst, J. Mol. Catal. A Chem. 267 (1–2) (2007) 79–85.
[215] Z. Yang, C. Zhang, Adsorption and photocatalytic degradation of bilirubin on hydroxyapatite coatings with nanostructural surface, J. Mol. Catal. A Chem. 302 (1–2) (2009) 107–111.
[216] T. Mitsudome, Y. Mikami, H. Mori, S. Arita, T. Mizugaki, K. Jitsukawa, K. Kaneda, Supported silver nanoparticle catalyst for selective hydration of nitriles to amides in water, Chem. Commun. (22) (2009) 3258–3260.
[217] R. Bai, S. Wang, F. Mei, T. Li, G. Li, Synthesis of glycerol carbonate from glycerol and dimethyl carbonate catalyzed by KF modified hydroxyapatite, J. Ind. Eng. Chem. 17 (4) (2011) 777–781.
[218] A. Fihri, C. Len, R.S. Varma, A. Solhy, Hydroxyapatite: a review of syntheses, structure and applications in heterogeneous catalysis, Coord. Chem. Rev. 347 (2017) 48–76.
[219] D. Zhang, H. Zhao, X. Zhao, Y. Liu, H. Chen, L. Xianjun, Application of hydroxyapatite as catalyst and catalyst carrier, Prog. Chem. 23 (4) (2011) 687–694.

[220] M. Othmani, H. Bachoua, Y. Ghandour, A. Aissa, M. Debbabi, Synthesis, characterization and catalytic properties of copper-substituted hydroxyapatite nanocrystals, Mater. Res. Bull. 97 (2018) 560–566.
[221] M. Schiavoni, S. Campisi, P. Carniti, A. Gervasini, T. Delplanche, Focus on the catalytic performances of Cu-functionalized hydroxyapatites in NH_3-SCR reaction, Appl. Catal. A Gen. 563 (2018) 43–53.
[222] J. Dobosz, M. Cichy, M. Zawadzki, T. Borowiecki, Glycerol steam reforming over calcium hydroxyapatite supported cobalt and cobalt-cerium catalysts, J. Energy Chem. 27 (2) (2018) 404–412.
[223] T.S. Phan, A.R. Sane, B. Rêgo de Vasconcelos, A. Nzihou, P. Sharrock, D. Grouset, D. Pham Minh, Hydroxyapatite supported bimetallic cobalt and nickel catalysts for syngas production from dry reforming of methane, Appl. Catal. B Environ. 224 (2018) 310–321.
[224] X. Zhang, M.Z. Yates, Controllable synthesis of hydroxyapatite-supported palladium nanoparticles with enhanced catalytic activity, Surf. Coat. Technol. 351 (2018) 60–67.
[225] X. Zhang, M.Z. Yates, Enhanced photocatalytic activity of TiO_2 nanoparticles supported on electrically polarized hydroxyapatite, ACS Appl. Mater. Interfaces 10 (20) (2018) 17232–17239.
[226] J. Kamieniak, P.J. Kelly, A.M. Doyle, C.E. Banks, Influence of the metal/metal oxide redox cycle on the catalytic activity of methane oxidation over Pd and Ni doped hydroxyapatite, Catal. Commun. 107 (2018) 82–86.
[227] Z. Boukha, M. Gil-Calvo, B. de Rivas, J.R. González-Velasco, J.I. Gutiérrez-Ortiz, R. López-Fonseca, Behaviour of Rh supported on hydroxyapatite catalysts in partial oxidation and steam reforming of methane: on the role of the speciation of the Rh particles, Appl. Catal. A Gen. 556 (2018) 191–203.
[228] Z. Xiong, Z. Yang, Y. Zhu, F. Chen, R. Yang, D. Qin, Ultralong hydroxyapatite nanowire-based layered catalytic paper for highly efficient continuous flow reactions, J. Mater. Chem. A 6 (14) (2018) 5762–5773.
[229] N. Elazarifi, A. Ezzamarty, J. Leglise, L.C. de Ménorval, C. Moreau, Kinetic study of the condensation of benzaldehyde with ethylcyanoacetate in the presence of Al-enriched fluoroapatites and hydroxyapatites as catalysts, Appl. Catal. A Gen. 267 (1) (2004) 235–240.
[230] N.S. Resende, M. Nele, V.M.M. Salim, Effects of anion substitution on the acid properties of hydroxyapatite, Thermochim. Acta 451 (1) (2006) 16–21.
[231] T. Tsuchida, J. Kubo, T. Yoshioka, S. Sakuma, T. Takeguchi, W. Ueda, Reaction of ethanol over hydroxyapatite affected by Ca/P ratio of catalyst, J. Catal. 259 (2) (2008) 183–189.
[232] L. Silvester, J.F. Lamonier, R.N. Vannier, C. Lamonier, M. Capron, A.S. Mamede, F. Pourpoint, A. Gervasini, F. Dumeignil, Structural, textural and acid–base properties of carbonate-containing hydroxyapatites, J. Mater. Chem. A 2 (29) (2014) 11073–11090.
[233] V.C. Ghantani, S.T. Lomate, M.K. Dongare, S.B. Umbarkar, Catalytic dehydration of lactic acid to acrylic acid using calcium hydroxyapatite catalysts, Green Chem. 15 (5) (2013) 1211–1217.
[234] S. Ogo, A. Onda, Y. Iwasa, K. Hara, A. Fukuoka, K. Yanagisawa, 1-Butanol synthesis from ethanol over strontium phosphate hydroxyapatite catalysts with various Sr/P ratios, J. Catal. 296 (2012) 24–30.
[235] A. Solhy, W. Amer, M. Karkouri, R. Tahir, A. El Bouari, A. Fihri, M. Bousmina, M. Zahouily, Bi-functional modified-phosphate catalyzed the synthesis of α-α'-(EE)-bis(benzylidene)-cycloalkanones: microwave versus conventional-heating, J. Mol. Catal. A Chem. 336 (1) (2011) 8–15.
[236] X. Li, L. Sun, W. Zou, P. Cao, Z. Chen, C. Tang, L. Dong, X. Li, L. Sun, W. Zou, Efficient conversion of bio-lactic acid to 2,3-pentanedione on cesium doped hydroxyapatite catalysts with balanced acid-base sites, ChemCatChem 9 (2017) 4621–4627.

[237] N. Viswanadham, S. Debnath, P. Sreenivasulu, D. Nandan, S.K. Saxena, A.H. Al-Muhtaseb, Nano porous hydroxyapatite as a bi-functional catalyst for bio-fuel production, RSC Adv. 5 (83) (2015) 67380–67383.
[238] N.Y. Siavashi, B. Akhlaghinia, M. Zarghani, Sulfonated nanohydroxyapatite functionalized with 2-aminoethyl dihydrogen phosphate (HAP@AEPH$_2$-SO$_3$H) as a reusable solid acid for direct esterification of carboxylic acids with alcohols, Res. Chem. Intermed. 42 (6) (2016) 5789–5806.
[239] M. Zarghani, B. Akhlaghinia, Sulfonated nanohydroxyapatite functionalized with 2-aminoethyl dihydrogen phosphate (HAP@AEPH$_2$-SO$_3$H) as a new recyclable and eco-friendly catalyst for rapid one-pot synthesis of 4,4′-(aryl methylene)bis(3-methyl-1H-pyrazol-5-ol)s, RSC Adv. 5 (107) (2015) 87769–87780.
[240] S.C. Oh, J. Xu, D.T. Tran, B. Liu, D. Liu, Effects of controlled crystalline surface of hydroxyapatite on methane oxidation reactions, ACS Catal. 8 (5) (2018) 4493–4507.
[241] I.Y. Jeon, J.B. Baek, Nanocomposites derived from polymers and inorganic nanoparticles, Materials 3 (6) (2010) 3654–3674.
[242] Y. Zuo, Y. Li, J. Li, X. Zhang, H. Liao, Y. Wang, W. Yang, Novel bio-composite of hydroxyapatite reinforced polyamide and polyethylene: composition and properties, Mater. Sci. Eng. A 452 (2007) 512–517.
[243] J. Russias, E. Saiz, R. Nalla, K. Gryn, R. Ritchie, A. Tomsia, Fabrication and mechanical properties of PLA/HA composites: a study of in vitro degradation, Mater. Sci. Eng. C Biomim. Supramol. Syst. 26 (8) (2006) 1289–1295.
[244] M. Dalby, L. Di Silvio, E. Harper, W. Bonfield, In vitro evaluation of a new polymethylmethacrylate cement reinforced with hydroxyapatite, J. Mater. Sci. Mater. Med. 10 (12) (1999) 793–796.
[245] Z. Hong, P. Zhang, A. Liu, L. Chen, X. Chen, X. Jing, Composites of poly (lactide-co-glycolide) and the surface modified carbonated hydroxyapatite nanoparticles, J. Biomed. Mater. Res. A 81 (3) (2007) 515–522.
[246] N. Sultana, M. Wang, PHBV/PLLA-based composite scaffolds fabricated using an emulsion freezing/freeze-drying technique for bone tissue engineering: surface modification and in vitro biological evaluation, Biofabrication 4 (1) (2012) 015003.
[247] A. Salerno, S. Zeppetelli, E. Di Maio, S. Iannace, P. Netti, Processing/structure/property relationship of multi-scaled PCL and PCL-HA composite scaffolds prepared via gas foaming and NaCl reverse templating, Biotechnol. Bioeng. 108 (4) (2011) 963–976.
[248] M. Dessì, M.G. Raucci, S. Zeppetelli, L. Ambrosio, Design of injectable organic–inorganic hybrid for bone tissue repair, J. Biomed. Mater. Res. A 100 (8) (2012) 2063–2070.
[249] M.G. Raucci, V. Guarino, L. Ambrosio, Hybrid composite scaffolds prepared by sol–gel method for bone regeneration, Compos. Sci. Technol. 70 (13) (2010) 1861–1868.
[250] D.O. Costa, S.J. Dixon, A.S. Rizkalla, One-and three-dimensional growth of hydroxyapatite nanowires during sol–gel–hydrothermal synthesis, ACS Appl. Mater. Interfaces 4 (3) (2012) 1490–1499.
[251] D. Yang, Y. Jin, G. Ma, X. Chen, F. Lu, J. Nie, Fabrication and characterization of chitosan/PVA with hydroxyapatite biocomposite nanoscaffolds, J. Appl. Polym. Sci. 110 (6) (2008) 3328–3335.
[252] S. Wang, L. Chen, Y. Tong, Structure-property relationship in chitosan-based biopolymer/montmorillonite nanocomposites, J. Polym. Sci. A Polym. Chem. 44 (1) (2006) 686–696.
[253] M. Aliabadi, M. Irani, J. Ismaeili, S. Najafzadeh, Design and evaluation of chitosan/hydroxyapatite composite nanofiber membrane for the removal of heavy metal ions from aqueous solution, J. Taiwan Inst. Chem. Eng. 45 (2) (2014) 518–526.
[254] E. Entcheva, H. Bien, L. Yin, C.Y. Chung, M. Farrell, Y. Kostov, Functional cardiac cell constructs on cellulose-based scaffolding, Biomaterials 25 (26) (2004) 5753–5762.

[255] Y. Wan, Y. Huang, C. Yuan, S. Raman, Y. Zhu, H. Jiang, F. He, C. Gao, Biomimetic synthesis of hydroxyapatite/bacterial cellulose nanocomposites for biomedical applications, Mater. Sci. Eng. C 27 (4) (2007) 855–864.
[256] C.J. Grande, F.G. Torres, C.M. Gomez, M.C. Bañó, Nanocomposites of bacterial cellulose/hydroxyapatite for biomedical applications, Acta Biomater. 5 (5) (2009) 1605–1615.
[257] S. Itoh, M. Kikuchi, K. Takakuda, Y. Koyama, H.N. Matsumoto, S. Ichinose, J. Tanaka, T. Kawauchi, K. Shinomiya, The biocompatibility and osteoconductive activity of a novel hydroxyapatite/collagen composite biomaterial, and its function as a carrier of rhBMP-2, J. Biomed. Mater. Res. 54 (3) (2001) 445–453.
[258] M. Kikuchi, H.N. Matsumoto, T. Yamada, Y. Koyama, K. Takakuda, J. Tanaka, Glutaraldehyde cross-linked hydroxyapatite/collagen self-organized nanocomposites, Biomaterials 25 (1) (2004) 63–69.
[259] M. Kikuchi, S. Itoh, S. Ichinose, K. Shinomiya, J. Tanaka, Self-organization mechanism in a bone-like hydroxyapatite/collagen nanocomposite synthesized in vitro and its biological reaction in vivo, Biomaterials 22 (13) (2001) 1705–1711.
[260] M. Azami, F. Orang, F. Moztarzadeh, Nanocomposite bone tissue-engineering scaffolds prepared from gelatin and hydroxyapatite using layer solvent casting and freeze-drying technique, in: International Conference on Biomedical and Pharmaceutical Engineering, 2006. ICBPE 2006, IEEE, 2006, pp. 259–264.
[261] M. Azami, M. Rabiee, F. Moztarzadeh, Glutaraldehyde crosslinked gelatin/hydroxyapatite nanocomposite scaffold, engineered via compound techniques, Polym. Compos. 31 (12) (2010) 2112–2120.
[262] S. Suganya, J. Venugopal, S. Ramakrishna, B. Lakshmi, V. Dev, Aloe vera/silk fibroin/hydroxyapatite incorporated electrospun nanofibrous scaffold for enhanced osteogenesis, J. Biomater. Tissue Eng. 4 (1) (2014) 9–19.
[263] B. Xiao, D.L. Zhou, W.Z. Yang, J. Ou, Y.J. Tang, H.Q. Chen, Preparation and characterization of porous Apatite-Wollastonite/β-Tricalcium phosphate composite scaffolds, J. Inorg. Mater. 2 (2006) 028.
[264] Y. Xu, F.W. Schwartz, Lead immobilization by hydroxyapatite in aqueous solutions, J. Contam. Hydrol. 15 (3) (1994) 187–206.
[265] D. Ghahremani, I. Mobasherpour, E. Salahi, M. Ebrahimi, S. Manafi, L. Keramatpour, Potential of nano crystalline calcium hydroxyapatite for Tin (II) removal from aqueous solutions: equilibria and kinetic processes, Arab. J. Chem. 10 (2017) S461–S471.
[266] Q.Y. Ma, S.J. Traina, T.J. Logan, J.A. Ryan, Effects of aqueous Al, Cd, Cu, Fe (II), Ni, and Zn on Pb immobilization by hydroxyapatite, Environ. Sci. Technol. 28 (7) (1994) 1219–1228.
[267] C. Shi, C. Lv, L. Wu, X. Hou, Porous chitosan/hydroxyapatite composite membrane for dyes static and dynamic removal from aqueous solution, J. Hazard. Mater. 338 (2017) 241–249.
[268] S.S. Metwally, I.M. Ahmed, H.E. Rizk, Modification of hydroxyapatite for removal of cesium and strontium ions from aqueous solution, J. Alloys Compd. 709 (2017) 438–444.
[269] W. Khanday, B. Hameed, Zeolite-hydroxyapatite-activated oil palm ash composite for antibiotic tetracycline adsorption, Fuel 215 (2018) 499–505.
[270] Y. Xu, F.W. Schwartz, S.J. Traina, Sorption of Zn^{2+} and Cd^{2+} on hydroxyapatite surfaces, Environ. Sci. Technol. 28 (8) (1994) 1472–1480.
[271] Y. Wang, L. Hu, G. Zhang, T. Yan, L. Yan, Q. Wei, B. Du, Removal of Pb (II) and methylene blue from aqueous solution by magnetic hydroxyapatite-immobilized oxidized multi-walled carbon nanotubes, J. Colloid Interface Sci. 494 (2017) 380–388.

[272] G. Rölla, H. Löe, C. Rindom Schiött, The affinity of chlorhexidine for hydroxyapatite and salivary mucins, J. Periodontal Res. 5 (2) (1970) 90–95.
[273] D.T.H. Wassell, R.C. Hall, G. Embery, Adsorption of bovine serum albumin onto hydroxyapatite, Biomaterials 16 (9) (1995) 697–702.
[274] A. Pandele, F. Comanici, C. Carp, F. Miculescu, S. Voicu, V. Thakur, B. Serban, Synthesis and characterization of cellulose acetate-hydroxyapatite micro and nano composites membranes for water purification and biomedical applications, Vacuum 146 (2017) 599–605.
[275] F. Gao, Q. Wang, N. Gao, Y. Yang, F. Cai, M. Yamane, F. Gao, H. Tanaka, Hydroxyapatite/chemically reduced graphene oxide composite: environment-friendly synthesis and high-performance electrochemical sensing for hydrazine, Biosens. Bioelectron. 97 (2017) 238–245.
[276] Z. He, L. He, C. Deng, Fibronectin adsorption on hydroxyapatite nanosensors and the effect of fibronectin preadsorption on biological apatite growth, J. Biomed. Nanotechnol. 14 (4) (2018) 736–746.
[277] P. Kanchana, N. Sudhan, C. Sekar, G. Neri, Manganese doped hydroxyapatite nanoparticles based enzyme-less electrochemical sensor for detecting hydroquinone, J. Nanosci. Nanotechnol. 19 (4) (2019) 2034–2043.
[278] P. Kanchana, M. Navaneethan, C. Sekar, Fabrication of Ce doped hydroxyapatite nanoparticles based non-enzymatic electrochemical sensor for the simultaneous determination of norepinephrine, uric acid and tyrosine, Mater. Sci. Eng. B 226 (2017) 132–140.
[279] F. Chen, Y. Zhu, F. Chen, L. Dong, R. Yang, Z. Xiong, Fire alarm wallpaper based on fire-resistant hydroxyapatite nanowire inorganic paper and graphene oxide thermosensitive sensor, ACS Nano 12 (4) (2018) 3159–3171.
[280] M. Mahabole, R. Aiyer, C. Ramakrishna, B. Sreedhar, R. Khairnar, Synthesis, characterization and gas sensing property of hydroxyapatite ceramic, Bull. Mater. Sci. 28 (6) (2005) 535–545.
[281] M. Nagai, T. Saeki, T. Nishino, Carbon dioxide sensor mechanism of porous hydroxyapatite ceramics, J. Am. Ceram. Soc. 73 (5) (1990) 1456–1460.
[282] R. Mene, M. Mahabole, R. Aiyer, R. Khairnar, Hydroxyapatite nanoceramic thick film: an efficient CO_2 gas sensor, Open Appl. Phys. J. 3 (2010) 10–16.
[283] R.S. Khairnar, S. Anjum, V. Kokol, M. Mahabole, Carbon nano tube doped nano-hydroxyapatite sensor matrix for gas sensing application, Int. J. Mod. Comm. Technol. Res. 2 (4) (2014) 29–34.
[284] B. Wang, J.J. Zhang, Z.Y. Pan, X.Q. Tao, H.S. Wang, A novel hydrogen peroxide sensor based on the direct electron transfer of horseradish peroxidase immobilized on silica–hydroxyapatite hybrid film, Biosens. Bioelectron. 24 (5) (2009) 1141–1145.
[285] M. Nagai, T. Nishino, T. Saeki, A new type of CO_2 gas sensor comprising porous hydroxyapatite ceramics, Sensors Actuators 15 (2) (1988) 145–151.
[286] A. Monkawa, T. Ikoma, S. Yunoki, T. Yoshioka, J. Tanaka, D. Chakarov, B. Kasemo, Fabrication of hydroxyapatite ultra-thin layer on gold surface and its application for quartz crystal microbalance technique, Biomaterials 27 (33) (2006) 5748–5754.
[287] G.C. Petrucelli, E.Y. Kawachi, L.T. Kubota, C.A. Bertran, Hydroxyapatite-based electrode: a new sensor for phosphate, Anal. Commun. 33 (7) (1996) 227–229.
[288] P. Kanchana, N. Lavanya, C. Sekar, Development of amperometric L-tyrosine sensor based on Fe-doped hydroxyapatite nanoparticles, Mater. Sci. Eng. C 35 (2014) 85–91.
[289] S. Anjum, V.N. Narwade, K.A. Bogle, R.S. Khairnar, Graphite doped hydroxyapatite nanoceramic: selective alcohol sensor, Nano-Struct Nano-Objects 14 (2018) 98–105.
[290] M. Sun, Z. Li, S. Wu, Y. Gu, Y. Li, Simultaneous detection of Pb^{2+}, Cu^{2+} and Hg^{2+} by differential pulse voltammetry at an indium tin oxide glass electrode modified by hydroxyapatite, Electrochim. Acta 283 (2018) 1223–1230.

[291] R. Yang, Y. Zhu, F. Chen, L. Dong, Z. Xiong, Luminescent, fire-resistant, and water-proof ultralong hydroxyapatite nanowire-based paper for multimode anticounterfeiting applications, ACS Appl. Mater. Interfaces 9 (30) (2017) 25455–25464.
[292] W. Gan, L. Gao, X. Zhan, J. Li, Hydrothermal synthesis of magnetic wood composites and improved wood properties by precipitation with $CoFe_2O_4$/hydroxyapatite, RSC Adv. 5 (57) (2015) 45919–45927.
[293] H. Li, D. Wu, J. Wu, L.Y. Dong, Y.J. Zhu, X. Hu, Flexible, high-wettability and fire-resistant separators based on hydroxyapatite nanowires for advanced lithium-ion batteries, Adv. Mater. 29 (44) (2017). 1703548.
[294] F. Chen, Y.J. Zhu, Large-scale automated production of highly ordered ultralong hydroxyapatite nanowires and construction of various fire-resistant flexible ordered architectures, ACS Nano 10 (12) (2016) 11483–11495.
[295] F. Chen, Y. Zhu, Z. Xiong, T. Sun, Y. Shen, Highly flexible superhydrophobic and fire-resistant layered inorganic paper, ACS Appl. Mater. Interfaces 8 (50) (2016) 34715–34724.
[296] H. Li, Y.J. Zhu, Y.Y. Jiang, Y.D. Yu, F. Chen, L.Y. Dong, J. Wu, Hierarchical assembly of monodisperse hydroxyapatite nanowires and construction of high-strength fire-resistant inorganic paper with high-temperature flexibility, ChemNanoMat 3 (4) (2017) 259–268.
[297] B.Z. Dholakiya, Use of non-traditional fillers to reduce flammability of polyester resin composites, polimeri 30 (1) (2009) 10–17.
[298] W. Guo, J. Liu, P. Zhang, L. Song, X. Wang, Y. Hu, Multi-functional hydroxyapatite/polyvinyl alcohol composite aerogels with self-cleaning, superior fire resistance and low thermal conductivity, Compos. Sci. Technol. 158 (2018) 128–136.
[299] S.B. Goodman, Z. Yao, M. Keeney, F. Yang, The future of biologic coatings for orthopaedic implants, Biomaterials 34 (13) (2013) 3174–3183.
[300] J. He, T. Huang, L. Gan, Z. Zhou, B. Jiang, Y. Wu, F. Wu, Z. Gu, Collagen-infiltrated porous hydroxyapatite coating and its osteogenic properties: in vitro and in vivo study, J. Biomed. Mater. Res. A 100 (7) (2012) 1706–1715.
[301] H. Daugaard, B. Elmengaard, J.E. Bechtold, T. Jensen, K. Soballe, The effect on bone growth enhancement of implant coatings with hydroxyapatite and collagen deposited electrochemically and by plasma spray, J. Biomed. Mater. Res. A 92 (3) (2010) 913–921.
[302] R. Asri, W. Harun, M.A. Hassan, S. Ghani, Z. Buyong, A review of hydroxyapatite-based coating techniques: sol–gel and electrochemical depositions on biocompatible metals, J. Mech. Behav. Biomed. Mater. 57 (2016) 95–108.
[303] J. Wang, Y. Chao, Q. Wan, Z. Zhu, H. Yu, Fluoridated hydroxyapatite coatings on titanium obtained by electrochemical deposition, Acta Biomater. 5 (5) (2009) 1798–1807.
[304] D. Sidane, H. Rammal, A. Beljebbar, S. Gangloff, D. Chicot, F. Velard, H. Khireddine, A. Montagne, H. Kerdjoudj, Biocompatibility of sol-gel hydroxyapatite-titania composite and bilayer coatings, Mater. Sci. Eng. C 72 (2017) 650–658.
[305] E.C.d.S. Rigo, J. Marchi, A.H.d.A. Bressiani, J.C. Bressiani, Hydroxyapatite coating on silicon nitride surfaces using the biomimetic method, Mater. Res. 11 (1) (2008) 47–50.
[306] A. Haider, S. Haider, S.S. Han, I.K. Kang, Recent advances in the synthesis, functionalization and biomedical applications of hydroxyapatite: a review, RSC Adv. 7 (13) (2017) 7442–7458.
[307] L. Hu, G. Zheng, J. Yao, N. Liu, B. Weil, M. Eskilsson, E. Karabulut, Z. Ruan, S. Fan, J.T. Bloking, Transparent and conductive paper from nanocellulose fibers, Energy Environ. Sci. 6 (2) (2013) 513–518.

[308] M. Kaushik, A. Moores, Nanocelluloses as versatile supports for metal nanoparticles and their applications in catalysis, Green Chem. 18 (3) (2016) 622–637.
[309] Y. Li, H. Zhu, H. Gu, H. Dai, Z. Fang, N.J. Weadock, Z. Guo, L. Hu, Strong transparent magnetic nanopaper prepared by immobilization of Fe_3O_4 nanoparticles in a nanofibrillated cellulose network, J. Mater. Chem. A 1 (48) (2013) 15278–15283.
[310] K. Benhamou, H. Kaddami, A. Magnin, A. Dufresne, A. Ahmad, Bio-based polyurethane reinforced with cellulose nanofibers: a comprehensive investigation on the effect of interface, Carbohydr. Polym. 122 (2015) 202–211.
[311] Y. Habibi, Key advances in the chemical modification of nanocelluloses, Chem. Soc. Rev. 43 (5) (2014) 1519–1542.
[312] J. Yuan, K. Laubernds, J. Villegas, S. Gomez, S.L. Suib, Spontaneous formation of inorganic paper-like materials, Adv. Mater. 16 (19) (2004) 1729–1732.
[313] B. Lu, Y. Zhu, F. Chen, Highly flexible and nonflammable inorganic hydroxyapatite paper, Chem Eur J 20 (5) (2014) 1242–1246.
[314] Z. Xiong, Z. Yang, Y. Zhu, F. Chen, Y. Zhang, R. Yang, Ultralong hydroxyapatite nanowires-based paper co-loaded with silver nanoparticles and antibiotic for long-term antibacterial benefit, ACS Appl. Mater. Interfaces 9 (27) (2017) 22212–22222.